*Inorg. Chem.* **2007**, *46*, 4887–4904


# Hydrothermal and Structural Chemistry of the Zinc(II)- and Cadmium(II)-1,2,4-Triazolate Systems

**Wayne Ouellette, Bruce S. Hudson, and Jon Zubieta***

*Department of Chemistry, Syracuse University, Syracuse, New York 13244*

Received November 29, 2006

Hydrothermal reactions of 1,2,4-triazole with zinc and cadmium salts have yielded 10 structurally unique materials of the M(II)/trz/$X^{n-}$ system, with M(II) = Zn and Cd and $X^{n-}$ = $F^-$, $Cl^-$, $Br^-$, $I^-$, $OH^-$, $NO_3^-$, and $SO_4^{2-}$ (trz = 1,2,4-triazolate). Of the zinc-containing phases, $[Zn(trz)_2]$ (**1**), $[Zn_2(trz)_3(OH)]\cdot 3H_2O$ (**3**$\cdot 3H_2O$), and $[Zn_2(trz)(SO_4)(OH)]$ (**4**) are three-dimensional, while [Zn(trz)Br] (**2**) is two-dimensional. All six cadmium phases, $[Cd_3(trz)_3F_2(H_2O)]\cdot 2.75H_2O$ (**5**$\cdot 2.75H_2O$), $[Cd_2(trz)_2Cl_2(H_2O)]$ (**6**), $[Cd_3(trz)_3Br_3]$ (**7**), $[Cd_2(trz)_3I]$ (**8**), $[Cd_3(trz)_5(NO_3)(H_2O)]\cdot H_2O$ (**9**$\cdot H_2O$), and $[Cd_8(trz)_4(OH)_2(SO_4)_5(H_2O)]$ (**10**), are three-dimensional. In all cases, the anionic components $X^{n-}$ participate in the framework connectivity as bridging ligands. The structural diversity of these materials is reflected in the variety of coordination polyhedra displayed by the metal sites: tetrahedral; trigonal bipyramidal; octahedral. Structures **3**, **5**, and **7**–**9** exhibit two distinct polyhedral building blocks. The materials are also characterized by a range of substructural components, including trinuclear and tetranuclear clusters, adamantoid cages, chains, layers, and complex frameworks.

Complex structures,[1−6] based on a molecular scale composite of inorganic and organic components, provide the potential for the design of novel functional materials for technological applications.[7] The inorganic component may confer useful magnetic or optical properties, mechanical hardness, and thermal stability, while the organic component offers processability, a potential for structural diversification, and a range of polarizabilities and luminescent properties.[8] The combination of the characteristics of the organic and inorganic components offers an opportunity to incorporate useful properties within a single composite, providing access to a vast area of complex, multifunctional materials.[9−23]

Representative examples of materials in which organic components exert significant structural control over inorganic microstructures include zeolites,[24−29] mesoporous oxides of

* To whom correspondence should be addressed. E-mail: jazubiet@syr.edu. Fax: 315-443-4070.

(1) Whitesides, G. M.; Ismagilov, R. F. *Science* **1999**, *284*, 89.
(2) Kiss, I. Z.; Hudson, J. L. *AICLE J.* **2003**, *49*, 2234.
(3) Lehn, J. M. *Proc. Natl. Acad. Sci. U.S.A.* **2002**, *99*, 4763.
(4) Lehn, J. M. *Science* **2002**, *295*, 2400.
(5) Förster, S.; Plantenberg, T. *Angew. Chem., Int. Ed.* **2002**, *41*, 688.
(6) Miller, A. D. *Chem. Biochem.* **2002**, *3*, 45.
(7) Janiak, C. *Dalton Trans.* **2003**, 2781 and references therein.
(8) Mitzi, D. B. *Dalton Trans.* **2001**, 1.
(9) Chen, B.; Ockwig, N. W.; Millward, A. R.; Contreras, S. D.; Yaghi, O. M. *Angew. Chem., Int. Ed.* **2005**, *44*, 4745.
(10) Roswell, J. L. C.; Yaghi, O. M. *Angew. Chem., Int. Ed.* **2005**, *44*, 4670.
(11) Bradshaw, D.; Claridge, J. B.; Cussen, E. J.; Prior, T. J.; Rosseinsky, M. J. *Chem. Res.* **2005**, *38*, 273−282.
(12) Rosseinsky, M. J. *Microporous Mesoporous Mater.* **2004**, *73*, 15−30.
(13) Cingolani, A.; Galli, S.; Masciocchi, N.; Pandolfo, L.; Pettinari, C.; Sironi, A. *J. Am. Chem. Soc.* **2005**, *127*, 6144.
(14) Ohmori, O.; Kawano, M.; Fujita, M. *Angew. Chem., Int. Ed.* **2005**, *44*, 1962.
(15) Lee, E. Y.; Jang, S. Y.; Suh, M. P. *J. Am. Chem. Soc.* **2005**, *127*, 6374.
(16) Noro, S.-I.; Kitagawa, S.; Kondo, M.; Seki, K. *Angew. Chem., Int. Ed.* **2000**, *39*, 2082.
(17) Wang, Z.; Zhang, B.; Kurmoo, M.; Green, M. A.; Fujiwara, H.; Otsuka, T.; Kobayashi, H. *Inorg. Chem.* **2005**, *44*, 1230.
(18) Kim, H.; Suh, M. P. *Inorg. Chem.* **2005**, *44*, 810.
(19) Sudik, A. C.; Millward, A. R.; Ockwig, N. W.; Cote, A. P.; Kim, J.; Yaghi, O. M. *J. Am. Chem. Soc.* **2005**, *127*, 7110.
(20) Kitaura, R.; Kitagawa, S.; Kubtoa, Y.; Kobayashi, T. C.; Kindo, K.; Mita, Y.; Matsuo, A.; Kobayashi, M.; Chang, H.-C.; Ozawa, T. C.; Suzuki, M.; Sakata, M.; Takata, M. *Science* **2002**, *298*, 2358.
(21) Bradshaw, D.; Prior, T. J.; Cussen, E. J.; Claridge, J. B.; Rosseinsky, M. J. *J. Am. Chem. Soc.* **2004**, *126*, 6106.
(22) Kepert, C. J.; Prior, T. J.; Rosseinsky, M. J. *J. Am. Chem. Soc.* **2000**, *122*, 5158.
(23) Halder, G. J.; Kepert, C. J.; Moubaraki, B.; Murray, K. S.; Cashion, J. D. *Science* (*Washington, D.C.)* **2002**, *298*, 1762.
(24) Breck, D. W. *Zeolite Molecular Sciences, Chemistry and Use*; Wiley and Sons: London, 1974.
(25) Szostak, R. *Molecular Series: Principles of Synthesis and Identification*; Van Nostrand Reinhold: New York, 1989.
(26) van Bekkum, H., Flanigan, E. M., Jansen, J. C., Jacobs, P. A., Eds. *Introduction to Zeolite Science and Practice*; Elsevier: Amsterdam, 1991.
(27) Armbruster, T.; Gunter, M. E. *Rev. Mineral. Geochem.* **2001**, *45*, 1.
(28) Balkus, K. J., Jr. *Prog. Inorg. Chem.* **2001**, *50*, 217.

10.1021/ic062269a CCC: $37.00 
Published on Web 05/12/2007

**Scheme 1**

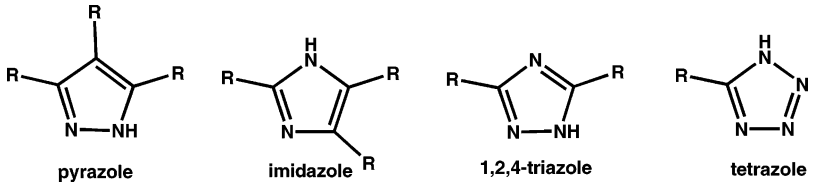


the MCM-41 class,[30−33] products of biomineralization,[31−36] transition metal phosphates with entrained organic cations,[37,38] and transition metal organophosphonates.[39−44] Since a common feature of such materials is the influence of the organic component in controlling the nucleation and growth of the inorganic oxide, one synthetic strategy exploits the synergism between organic and inorganic substructures in the sense that the organic component serves to imprint structural information onto the inorganic substructure, while in turn the coordination requirements of the metal cations impose geometric constraints on the juxtapositions of the organic subunits, thus conferring a hierarchical coding of the chemistry. In this view, the inorganic and organic substructures are complementary building blocks bearing recognition information.

One design strategy for organic−inorganic hybrid materials exploits the metal components as nodes, which are interconnected through appropriate organic tethers.[45,46] Carboxylates, polypyridines, and organophosphonates have witnessed the most significant development as components of such materials.[47−54] However, other ligands can afford different tether lengths, different charge-balance requirements, and alternative functional group orientations. While

**Scheme 2**

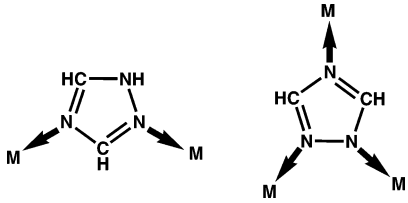

five-membered heterocycles of which pyrazole, imidazole, triazole, and tetrazole are representative are small and simple organic ligands, they are effective bridging ligands (Scheme 1).[55−66] Specifically, 1,2,4-triazole can function as a neutral bridging ligand to two metal sites or in the azolate form as a bridge to the three metal centers (Scheme 2). Triazole/triazolate is consequently an effective component in the design of binary metal/triazolate materials and ternary metal/triazolate/anion compounds. Furthermore, triazoles are readily derivatized, and a large number of functionalized compounds are readily accessible. The superexchange capacity of the ligand also endows unusual magnetic properties to the complexes, as we and others have noted.[67−72]


(29) van Steen, E., Claeys, M., Callanan, L. H., Eds. Recent advances in science and technology of zeolites and related materials. Proceedings of the 14th International Conference, Cape Town, South Africa, Apr 25−30, 2004. *Stud. Surf. Sci. Catal.* **2004**, 154C.
(30) Kresge, C. T.; Leonowicz, M. E.; Roth, W. J.; Vartuli, J. C.; Beck, J. S. *Nature* **1992**, *359*, 710.
(31) Selvam, P.; Bhatia, S. K.; Sonwane, C. G. *Ind. Eng. Chem. Res.* **2001**, *40*, 3237.
(32) Biz, S.; Occelli, M. L. *Catal. Rev.−Sci. Eng.* **1998**, *40*, 329.
(33) Kresge, C. T.; Vartuli, J. C.; Roth, W. J.; Leonowicz, M. E. *Stud. Surf. Sci. Catal.* **2004**, *148 (Mesoporous Crystals and Related Nano-Structured Materials)*, 53.
(34) Constantz, B. R. *Nanoscale Technol. Biol. Syst.* **2005**, 217.
(35) Estroff, L. A.; Hamilton, A. D. *Chem. Mater.* **2001**, *13*, 3227.
(36) *Biomineralization: from biology to biotechnology and medical application*; Baeuerlein, E., Ed.; Wiley: Weinheim, Germany, 2001.
(37) Choudhury, A.; Rao, C. N. R. *Chem. Commun.* **2003**, 366.
(38) Finn, R. C.; Haushalter, R. C.; Zubieta, J. *Prog. Inorg. Chem.* **2003**, *51*, 421.
(39) Vioux, A.; LeBideau, J.; Mutin, P. H.; Leclercq, D. *Top. Curr. Chem.* **2004**, *232*, 145.
(40) Clearfield, A. *Curr. Opin. Solid State Mater. Sci.* **2003**, *6*, 495.
(41) Clearfield, A. *Prog. Inorg. Chem.* **1998**, *47*, 371.
(42) Alberti, G. In *Comprehensive Supramolecular Chemistry*; Atwood, J. L., Davis, J. E. D., Vogel, F., Eds.; Pergamon Press: New York, 1996; Vol. 9 (Alberti, G., Bein, T., Eds.), p 152.
(43) Kong, D.; Clearfield, A. *Chem. Commun.* **2005**, 1005.
(44) Kong, D.; Zon, J.; McBee, J.; Clearfield, A. *Inorg. Chem.* **2006**, *45*, 977 and references therein.
(45) Kitagawa, S.; Noro, S. *Compr. Coord. Chem. 2* **2004**, *7*, 231.
(46) Yaghi, O. M.; O'Keeffe, M.; Ockwig, N. W.; Chae, H. K.; Eddaoudi, M.; Kim, J. *Nature* **2003**, *423*, 705.
(47) James, S. L. *Chem. Soc. Rev.* **2003**, *32*, 276.
(48) Rao, C. N. R.; Natarajan, S.; Vaidhyanathan, R. *Angew. Chem., Int. Ed.* **2004**, *43*, 1466.
(49) Kitagawa, S.; Kitaura, R.; Noro, S.-I. *Angew. Chem., Int. Ed.* **2004**, *43*, 2334.
(50) Papaefstathiou, G. S.; MacGillivray, L. R. *Coord. Chem. Rev.* **2003**, *246*, 169.
(51) Eddaoudi, M.; Moler, D. B.; Li, H.; Chen, B.; Reineke, T. M.; O'Keeffe, M.; Yaghi, O. M. *Acc. Chem. Res.* **2001**, *34*, 319.
(52) Clearfield, A.; Sharma, C. V. K.; Zhang, B. *Chem. Mater.* **2001**, *13*, 3099.
(53) Mellot-Draznieks, C.; Ferey, G. *Prog. Solid State Chem.* **2006**, *33*, 187.
(54) Ferey, G. *Chem. Mater.* **2001**, *13*, 3084.
(55) Zhang, J.-P.; Chen, X.-M. *Chem. Commun.* **2006**, 1689.
(56) Potts, K. T. *Chem. Rev.* **1961**, *61*, 87.
(57) Klingale, M. H.; Brooker, S. *Coord. Chem. Rev.* **2003**, *241*, 119.
(58) Beckman, U.; Brooker, S. *Coord. Chem. Rev.* **2003**, *245*, 17.
(59) Haasnoot, J. G. *Coord. Chem. Rev.* **2000**, *131*, 200−202.
(60) Chivers, T.; Fu, Z.; Thompson, L. K. *Chem. Commun.* **2005**, 2339.
(61) Zhang, J.-P.; Lin, Y.-Y.; Huang, X.-C.; Chen, X.-M. *J. Am. Chem. Soc.* **2005**, *127*, 5495.
(62) Zhang, J.-P.; Zhang, S.-L.; Huang, X.-C.; Chen, X.-M. *Angew. Chem., Int. Ed.* **2004**, *43*, 206.
(63) Ferrer, S.; Lloret, F.; Bertomeu, I.; Alzuet, G.; Borras, J.; Garcia-Granda, S.; Liu-Gonzalez, M.; Haasnoot, J. G. *Inorg. Chem.* **2002**, *41*, 5821.
(64) Zhou, J.-H.; Cheng, R.-M.; Song, Y.; Li, Y.-Z.; Yu, Z.; Chen, X.-T.; Xue, Z.-L.; You, X.-Z. *Inorg. Chem.* **2005**, *44*, 8011.
(65) Du, M.; Jiang, X.-J.; Zhao, X.-J. *Chem. Commun.* **2005**, 5521.
(66) Zhang, J.-P.; Lin, Y.-Y.; Zhang, W.-X.; Chen, X.-M. *J. Am. Chem. Soc.* **2005**, *127*, 14162.
(67) Ouellette, W.; Yu, M.-H.; O'Connor, C. J.; Hagrman, D.; Zubieta, J. *Angew. Chem., Int. Ed.* **2006**, *45*, 3497.
(68) Ouellette, W.; Galan-Mascaros, J. R.; Dunbar, K. R.; Zubieta, J. *Inorg. Chem.* **2006**, *45*, 1909.
(69) Hagrman, P. J.; Bridges, C.; Greedan, J. E.; Zubieta, J. *J. Chem. Soc., Dalton Trans.* **1999**, 2901.
(70) Kahn, O.; Martinez, C. J. *Science* **1998**, *279*, 44 and references therein.
(71) Klingele, M. H.; Boyd, P. D. W.; Moubaraki, B.; Murray, K. S.; Brooker, S. *Eur. J. Inorg. Chem.* **2005**, 910.
(72) Ferrer, S.; van Korringsbruggen, P. J.; Haasnoot, J. G.; Reedijk, J.; Kooijman, H.; Spek, A. L.; Lezama, L.; Arif, A. M.; Miller, J. S. *J. Chem. Soc., Dalton Trans.* **1999**, 4269.

In addition to providing structural diversity and unusual magnetochemistry, the azolates also allow the design of materials with interactions between closed-shell $d^{10}$ metal cations, providing a route to new luminescent materials. A number of binary Cu(I)/pyrazolates and Cu(I)/triazolates with photoluminescent properties have been described.[61,73,74] More recently, we demonstrated that the ternary Cu(I)/trz/anion system also provided a series of materials with bright phosphorescence and luminescent thermochromism. As an extension of this work, the ternary phrases M(II)/trz/anion for M = Zn and Cd have been investigated. The three-dimensional structures of $[Zn(trz)_2]$ (**1**), $[Zn_2(trz)_3(OH)]\cdot 3H_2O$ (**3**$\cdot 3H_2O$), $[Zn_2(trz)(SO_4)(OH)]$ (**4**), $[Cd_3(trz)_3F_2(OH)]\cdot 3H_2O$ (**5**$\cdot 3H_2O$), $[Cd_2(trz)_2Cl_2(H_2O)]$ (**6**), $[Cd_3(trz)_3Br_3]$ (**7**), $[Cd_2(trz)_3I]$ (**8**), $[Cd_3(trz)_5(NO_3)(H_2O)]\cdot H_2O$ (**9**$\cdot H_2O$), and $[Cd_8(trz)_4(OH)_2(SO_4)_5(H_2O)]$ (**10**) are reported, as well as the two-dimensional structure of [Zn(trz)Br] (**2**).

## Experimental Section

**General Considerations.** All chemicals were used as obtained without further purification: zinc oxide, zinc nitrate hexahydrate, zinc sulfate heptahydrate, zinc bromide, cadmium fluoride, cadmium chloride hemipentahydrate, cadmium bromide, cadmium iodide, cadmium nitrate tetrahydrate, cadmium sulfate hydrate, 1,2,4-triazole, and tetrabutylammoniumhydroxide were purchased from Aldrich. All syntheses were carried out in 23 mL poly(tetrafluoroethylene) lined stainless steel containers under autogenous pressure. The reactants were stirred briefly, and the initial pH was measured before heating. Water was distilled above 3.0 M Ω in-house using a Barnstead model 525 Biopure distilled water center. The reactions' initial and final pH values were measuered using Hydrion pH sticks.

**Synthesis of $[Zn(trz)_2]$ (1).** A mixture of ZnO (0.142 g, 1.745 mmol), 1,2,4-triazole (0.234 g, 3.388 mmol), and $H_2O$ (10.00 g, 556 mmol) in the mol ratio 0.52:1.00:164 was stirred briefly before heating to 200 °C for 48 h, with initial and final pH values of of 5.0 and 6.0. Colorless blocks of **1,** suitable for X-ray diffraction, were isolated in 85%. IR (KBr pellet, $cm^{-1}$): 3139 (m), 1508 (s), 1458 (w), 1346 (w), 1312 (w), 1275 (s), 1205 (w), 1159 (s), 1070 (m), 1004 (m), 883 (w), 664 (s).

**Synthesis of [Zn(trz)Br] (2).** A mixture of $ZnBr_2$ (0.391 g, 1.736 mmol), 1,2,4-triazole (0.238 g, 3.446 mmol), and $H_2O$ (10.00 g, 556 mmol) in the mol ratio 0.50:1.00:161 was stirred briefly before heating to 200 °C for 48 h. Initial and final pH values of 2.5 and 3.0, respectively, were recorded. Colorless rods of **2** suitable for X-ray diffraction were isolated in 80% yield. IR (KBr pellet, $cm^{-1}$): 3129 (w), 3108 (m), 3041 (w), 2943 (w), 1528 (s), 1330 (w), 1302 (s), 1217 (w), 1177 (m), 1096 (s), 1042 (m), 1005 (m), 902 (w), 884 (m), 658 (s).

**Synthesis of $[Zn_2(trz)_3(OH)]\cdot 3H_2O$ (3**$\cdot 3H_2O$**).** A solution of $Zn(NO_3)_2\cdot 6H_2O$ (0.478 g, 1.607 mmol), 1,2,4-triazole (0.233 g, 3.373 mmol), and $H_2O$ (10.00 g, 556 mmol) in the mol ratio 0.48:1.00:165 was stirred briefly before heating to 200 °C for 72 h (initial and final pH values of 4.0 and 3.0, respectively). Colorless blocks of **3**$\cdot 3H_2O$, suitable for X-ray diffraction, were isolated in 90% yield. IR (KBr pellet, $cm^{-1}$): 3127 (w), 1510 (s), 1458 (s), 1314 (s), 1276 (m), 1163 (s), 1077 (m), 1033 (m), 1009 (m), 894 (w), 817 (w), 663 (s).

**Synthesis of $[Zn_2(trz)(OH)(SO_4)]$ (4).** A solution of $ZnSO_4\cdot 7H_2O$ (0.462 g, 1.607 mmol), 1,2,4-triazole (0.232 g, 3.359 mmol), and $H_2O$ (10.00 g, 556 mmol) in the mol ratio 0.48:1.00:166 was stirred briefly before heating to 200 °C for 48 h (initial and final pH values of 4.5 and 7.5, respectively). Colorless crystals of **4** were isolated in 85% yield. IR (KBr pellet, $cm^{-1}$): 3430 (s), 3148 (m), 1560 (m), 1524 (m), 1292 (m), 1208 (m), 1174 (m), 1113 (s), 1077 (s), 1008 (m), 900 (m), 873 (m), 826 (m), 644 (m), 620 (m).

**Synthesis of $[Cd_3(trz)_3F_2(OH)]\cdot 3H_2O$ (5**$\cdot 3H_2O$**).** A solution of $CdF_2$ (0.249 g, 1.655 mmol), 1,2,4-triazole (0.234 g, 3.388 mmol), $H_2O$ (10.00 g, 556 mmol), and tetrabutylammonium hydroxide (40%) (0.250 mL, 0.385 mmol) in the mol ratio 0.49:1.00:164:0.11 was stirred briefly before heating to 180 °C for 72 h (initial and final pH values of 5.5 and 3.5, respectively). Colorless crystals of **5**$\cdot 3H_2O$, suitable for X-ray diffraction, were isolated in 90% yield. IR (KBr pellet, $cm^{-1}$): 3100 (b), 1751 (m), 1508 (s), 1403 (m), 1325 (m), 1284 (s), 1197 (m), 1155 (s), 1069 (s), 1016 (m), 991 (s), 881 (m), 664 (s).

**Synthesis of $[Cd_2(trz)_2Cl_2(H_2O)]$ (6).** A solution of $CdCl_2\cdot 2.5H_2O$ (0.290 g, 1.270 mmol), 1,2,4-triazole (0.237 g, 3.431 mmol), and $H_2O$ (10.00 g, 556 mmol) in the mol ratio 0.37:1.00:162 was stirred for 10 min before heating to 200 °C for 96 h (initial and final pH values of 5.0 and 4.5, respectively). Colorless plates of **6** were isolated in 65% yield. IR (KBr pellet, $cm^{-1}$): 3590 (s), 3400 (s), 3132 (w), 1753 (w), 1598 (w), 1560 (w), 1501 (s), 1283 (s), 1190 (w), 1155 (s), 1062 (m), 1010 (w), 992 (m), 881 (m), 662 (m).

**Synthesis of $[Cd_3(trz)_3Br_3]$ (7).** A mixture of $CuBr_2$ (0.577 g, 1.676 mmol), 1,2,4-triazole (0.233 g, 3.373 mmol), $H_2O$ (10.00 g, 556 mmol), and tetrabutylammonium hydroxide (40%) (0.250 mL, 0.385 mmol) in the mol ratio 0.50:1.00:165:0.11 was stirred briefly before heating to 200 °C for 48 h. Initial and final pH values of 4.5 and 3.0, respectively, were recorded. Colorless plates of **7** suitable for X-ray diffraction were isolated in 75% yield. IR (KBr pellet, $cm^{-1}$): 3245 (b), 3123 (w), 2996 (w), 1734 (w), 1638 (w), 1542 (m), 1508 (s), 1409 (m), 1299 (m), 1279 (s), 1159 (s), 1123 (w), 1079 (s), 1045 (m), 998 (w), 988 (m), 968 (w), 875 (m), 699 (m), 666 (m), 653 (m), 623 (s).

**Synthesis of $[Cd_2(trz)_3I]$ (8).** A solution of $CdI_2$ (0.613 g, 1.674 mmol), 1,2,4-triazole (0.235 g, 3.402 mmol), and $H_2O$ (10.00 g, 556 mmol) in the mol ratio 0.49:1.00:163 was stirred briefly before heating to 180 °C for 48 h (initial and final pH values of 4.0 and 3.0, respectively). Colorless rods of **8** suitable for X-ray diffraction were isolated in 70% yield. IR (KBr pellet, $cm^{-1}$): 3233 (b), 3123 (w), 2994 (w), 2892 (w), 1535 (w), 1502 (s), 1411 (w), 1301 (m), 1275 (m), 1153 (s), 1121 (m), 1069 (m), 1046 (m), 996 (w), 870 (w), 660 (m), 616 (s).

**Synthesis of $[Cd_3(trz)_5(NO_3)(H_2O)]\cdot H_2O$ (9**$\cdot H_2O$**).** A solution of $Cd(NO_3)_2\cdot 4H_2O$ (0.491 g, 1.592 mmol), 1,2,4-triazole (0.233 g, 3.373 mmol), and $H_2O$ (10.00 g, 556 mmol) in the mol ratio 0.47:1.00:165 was heated at 200 °C for 96 h (initial and final pH values of 4.5 and 4.5, respectively). Colorless blocks of **9**$\cdot H_2O$ were isolated in 85% yield. IR (KBr pellet, $cm^{-1}$): 3567 (b), 3233 (b), 3123 (w), 2994 (w), 2892 (w), 1535 (w), 1502 (s), 1411 (w), 1301 (m), 1275 (m), 1153 (s), 1121 (m), 1069 (m), 1046 (m), 996 (w), 870 (w), 660 (m), 616 (s).

**Synthesis of $[Cd_8(trz)_4(SO_4)_5(OH)_2(H_2O)]$ (10).** A mixture of $CdSO_4\cdot 8H_2O$ (0.430 g, 0.559 mmol), 1,2,4-triazole (0.232 g, 3.359 mmol), $H_2O$ (10.00 g, 556 mmol), and tetrabutylammonium hydroxide (40%) (0.075 mL, 0.116 mmol) in the mol ratio 0.17:

(73) Dias, H. V. R.; Diyabalange, H. V. K.; Eldabaja, M. G.; Elbjeirami, O.; Rawashdeh-Omary, M. A.; Omary, M. A. *J. Am. Chem. Soc.* **2005**, *127*, 7489.
(74) Omary, M. A.; Rawashdeh-Omary, M. A.; Gonser, M. W. A.; Elbjeirami, O.; Grimes, T.; Cundair, T. R. *Inorg. Chem.* **2005**, *44*, 8200.

1.00:768:0.03 was stirred for 20 min before heating to 200 °C for 48 h. Initial and final pH values of 4.5 and 3.0, respectively, were recorded. Colorless crystals of **10** suitable for X-ray diffraction were isolated in 65% yield. IR (KBr pellet, $cm^{-1}$): 3487 (b), 3141 (w), 1654 (m), 1637 (m), 1508 (s), 1284 (m), 1156 (s), 1117 (s), 1061 (s), 990 (m), 874 (m), 799 (m), 739 (w), 666 (m), 613 (m).

**X-ray Crystallography.** Structural measurements were performed on a Bruker-AXS SMART-CCD diffractometer at low temperature (90 K) using graphite-monochromated Mo Kα radiation ($\lambda_{Mo\ K\alpha} = 0.710\ 73$ Å).[75] The data were corrected for Lorentz and polarization effects and absorption using SADABS.[76,77] The structures were solved by direct methods. All non-hydrogen atoms were refined anisotropically. After all of the non-hydrogen atoms were located, the model was refined against $F^2$, initially using isotropic and later anisotropic thermal displacement parameters. Hydrogen atoms were introduced in calculated positions and refined isotropically. Neutral atom scattering coefficients and anomalous dispersion corrections were taken from the *International Tables*, Vol. C. All calculations were performed using SHELXTL crystallographic software packages.[78]

Crystallographic details have been summarized in Table 1. Atomic positional parameters, full tables of bond lengths and angles, and anisotropic temperature factors are available in the Supporting Information. Selected bond lengths and angles are given in Table 2.

**Gas and Vapor Sorption Measurements.** All gas and vapor adsorption measurements were obtained using a Micromeritics ASAP 2020 volumetric gas adsorption instrument equipped with a vapor dosing attachment. The crystalline sample of $[Zn(trz)F]\cdot H_2O$ was evacuated under dynamic vacuum at 160 °C at a heating rate of 0.1 °C/min until the outgas rate was less than 2 mTorr/min. For all isotherms, warm and cold free space correction measurements were taken using ultrahigh-purity helium gas. The $H_2$ and $N_2$ isotherms at 77 K were measured in liquid-nitrogen baths using UHP grade gas sources. The methanol isotherm measurements at 298 K were performed in a constant temperature bath using triple distilled and degassed methanol.

**DFT Calculations.** Solid-state density functional theory (DFT) calculations[79] were performed with the program DMol$^3$ to calculate the electronic band structure of [Zn(trz)Cl]. DMol$^3$ solid-state calculations were performed with the program option set to "fine" (corresponding to a *k*-point separation of 0.04 $Å^{-1}$) and the energy convergence of $1 \times 10^{-6}$ hartree, the dnp (double numerical with p and d polarization) basis set (comparable to a 6-31G(d,P) Gaussian-type basis set), and the VWN-BP generalized gradient approximation (GGA) density functional. Unlike many plane-wave DFT packages, Dmol$^3$ does not optimize lattice constants, such that the atoms within the unit cell were optimized with the cell parameters specified by the 90 K X-ray diffraction study.

## Results and Discussion

**Syntheses and Infrared Spectroscopy.** Although metal−triazolate-based materials have excited considerable attention in recent years, the polymeric phases generally occur as insoluble and intractable polycrystalline powders. The expedient of hydrothermal reaction conditions affords a convenient method for the preparation of single crystals, allowing more routine structural characterization by single-crystal X-ray diffraction.[55] The techniques of hydrothermal, and more generally solvatothermal synthesis, have been well-established for the preparation of metal oxides and organic−inorganic composite materials.[80,81] The product composition may depend on critical factors such as pH of the medium, temperature, and hence pressure, as well as the presence of potential charge balancing anions which may also be incorporated into the product. In the series of materials described in this contribution, a charge-balancing inorganic anion is incorporated in all cases, with the exception of the binary material $[Zn(trz)_2]$ (**1**). In all compounds of this study, as well as the previously described Cu/trz/X materials,[82] the heterocyclic ligand is present in the deprotonated triazolate form and functions as a tridentate bridging group.

The hydrothermal chemistry of the zinc and cadmium triazolates is generally characterized by the incorporation of anionic component of the metal salt into the final product. The exceptions are $[Zn(trz)_2]$ (**1**), which was prepared from ZnO, and $[Zn_2(trz)_3(OH)]\cdot 3H_2O$ (**3**·$3H_2O$), which failed to incorporate the nitrate anion of the starting material $Zn(NO_3)_2\cdot 6H_2O$. Despite repeated attempts, no conditions could be found that provided Zn/trz/$NO_3^-$ phases. Similarly, we were unable to prepare crystalline products of the Zn/trz/$I^-$ composition. The use of $ZnCl_2$ resulted in the previously reported [Zn(trz)Cl],[83] while the reaction of $ZnF_2\cdot 4H_2O$ with 1,2,4-triazole yielded the known phase $[Zn(trz)F]\cdot H_2O$.[84] In contrast, the cadmium series afforded crystalline materials with X = $F^-$, $Cl^-$, Br, and $I^-$ as well as $NO_3^-$ and $SO_4^{2-}$.

It is also noteworthy that incorporation of coordinated water and/or hydroxide ligands is quite common, as evident in compounds **3**−**6**, **9**, and **10**. However, the hydroxide-containing phases were uniformly prepared from acidic solutions.

The infrared spectra of all compounds **1**−**10** exhibit a medium intensity band in the 3100−3160 $cm^{-1}$ range and a medium to strong band in the 1200−1290 $cm^{-1}$ range, associated with ν(C−H) and ν(C−N) or ν(N−N) of the triazolate ligand, respectively. The sulfate phases **4** and **10** exhibit characteristic ν(S−O) bands in the 1060−1075 and


(75) *SMART, Data Collection Software*, version 5.630; Bruker-AXS Inc.: Madison, WI, 1997.
(76) *SAINT Plus, Date Reduction Software*, version, 6.45A; Bruker-AXS Inc.: Madison, WI, 1997.
(77) Sheldrick, G. M. *SADABS*; University of Göttingen: Göttingen, Germany, 1996.
(78) *SHELXTL PC*, version 6.12; Bruker-AXS Inc.: Madison, WI, 2002.
(79) (a) Delley, B. *J. Chem. Phys.* **1990**, *92*, 508. (b) Delley, B. *J. Chem. Phys.* **2000**, *113*, 7756. (c) DMol$^3$ is available as part of Materials Studio.
(80) (a) Stein, A.; Keller, S. W.; Mallouk, T. E. *Science* **1993**, *259*, 1558. (b) Laudise, R. A. *Chem. Eng. News* **1987**, Sept 28, p 30. (c) Gopalakrishnan, J. *Chem. Mater.* **1995**, *7*, 1265. (d) Whittinghan, M. S. *Curr. Opin. Solid State Mater. Sci.* **1996**, *1*, 227. (e) Weller, M.; Dann, S. E. *Curr. Opin. Solid State Mater. Sci.* **1998**, *3*, 137. (f) Gopalakrishnan, J.; Bhuvanrh, N. S. P.; Rangan, K. K. *Curr. Opin. Solid State Mater. Sci.* **1996**, *1*, 285. (g) Rabenau, A. *Angew. Chem., Int. Ed. Engl.* **1985**, *24*, 1026. (h) Lobachev, A. N. *Crystallization processes under hydrothermal conditions*; Consultants Bureau: New York, 1973. (i) Yoshimura, M.; Suchanek, W. L.; Byrappa, K. *Mater. Res. Soc. Bull.* **2000**, *Sept*, 17. (j) Fing, S.; Xu, R. *Acc. Chem. Res.* **2001**, *34*, 239.
(81) Zubieta, J. *Compr. Coord. Chem. 2* **2003**, *1*, 697.
(82) Ouellette, W.; Prosvirin, A. V.; Chieffo, V.; Dunbar, K. R.; Hudson, B.; Zubieta, J. *Inorg. Chem.* **2006**, 0000.
(83) Kröber, J.; Bkouchi-Waksman, I.; Pascard, C.; Thomann, M.; Kahn, O. *Inorg. Chim. Acta* **1995**, *230*, 159.
(84) Goforth, A. M.; Su, C.-Y.; Mipp, R.; Macquart, R. B.; Smith, M. D.; Zur Loye, H.-C. *J. Solid State Chem.* **2005**, *178*, 2511.

**Table 1.** Summary of Crystallographic Data for the Structures of $[Zn(trz)_2]$ (**1**), [Zn(trz)Br] (**2**), $[Zn_2(trz)_3(OH)]\cdot 3H_2O$ (**3**·$3H_2O$), $[Zn_2(trz)(OH)(SO_4)]$ (**4**), $[Cd_3(trz)_3F_2(OH)]\cdot 3H_2O$ (**5**·$3H_2O$), $[Cd_2(trz)_2Cl_2(H_2O)]$ (**6**), $[Cd_3(trz)_3Br_3]$ (**7**), $[Cd_2(trz)_3I]$ (**8**), $[Cd_3(trz)_5(NO_3)(H_2O)]\cdot H_2O$ (**9**·$H_2O$), and $[Cd_8(trz)_4(SO_4)_5(OH)_2(H_2O)]$ (**10**)

| param | **1** | **2** | **3** | **4** |
|---|---|---|---|---|
| empirical formula | $C_4H_4N_6Zn$ | $C_2H_2BrN_3Zn$ | $C_3H_{6.50}N_{4.50}O_2Zn$ | $CH_{1.50}N_{1.50}O_{2.50}S_{0.50}$ Zn |
| fw | 203.52 | 213.35 | 203.00 | 155.94 |
| cryst syst | orthorhombic | monoclinic | orthorhombic | orthorhombic |
| space group | *Pbca* | $P2_1/n$ | *Pnma* | *Pnma* |
| *a*, Å | 9.9639(8) | 6.3341(6) | 7.5978(4) | 7.3183(4) |
| *b*, Å | 9.7061(8) | 9.6687(9) | 9.9695(5) | 6.8119(4) |
| *c*, Å | 14.1313(9) | 9.0805(8) | 17.5058(9) | 13.7846(7) |
| α, deg | 90 | 90 | 90 | 90 |
| *β*, deg | 90 | 102.888(2) | 90 | 90 |
| *γ*, deg | 90 | 90 | 90 | 90 |
| *V*,Å$^3$ | 1366.6(3) | 542.10(9) | 1326.00(12) | 687.18(7) |
| *Z* | 8 | 4 | 8 | 8 |
| $D_{calcd}$, g cm$^{-3}$ | 1.978 | 2.614 | 2.034 | 3.015 |
| $\mu$, mm$^{-1}$ | 3.528 | 11.764 | 3.651 | 7.275 |
| *T*, K | 90 | 90 | 90 | 90 |
| *λ*, Å | 0.710 73 | 0.710 73 | 0.710 73 | 0.710 73 |
| R1[a] | 0.0460 | 0.0185 | 0.0283 | 0.0250 |
| wR2[b] | **0.1161** | **0.0481** | **0.0704** | **0.0627** |

| param | **5** | **6** | **7** | **8** |
|---|---|---|---|---|
| empirical formula | $C_6H_{13}Cd_3F_2N_8O_4$ | $C_2H_3CdClN_3O_{0.50}$ | $C_6H_6Br_3Cd_3N_9$ | $C_3H_3CdI_{0.50}N_{4.50}$ |
| fw | 652.33 | 224.92 | 781.13 | 277.95 |
| cryst syst | orthorhombic | orthorhombic | monoclinic | orthorhombic |
| space group | *Ccca* | *Pnma* | $P2_1/c$ | *Pnma* |
| a, Å | 18.0700(6) | 7.5186(4) | 15.6858(11) | 7.8569(5) |
| *b*, Å | 18.0766(6) | 11.7796(6) | 12.5013(9) | 10.3906(6) |
| *c*, Å | 17.9952(6) | 12.3158(6) | 8.4003(6) | 18.5780(11) |
| α, deg | 90 | 90 | 90 | 90 |
| *β*, deg | 90 | 90 | 103.0910(10) | 90 |
| *γ*, deg | 90 | 90 | 90 | 90 |
| *V*, Å$^3$ | 5878.0(3) | 1090.76(10) | 1604.4(2) | 1516.67(16) |
| *Z* | 16 | 8 | 4 | 8 |
| $D_{calcd}$, g cm$^{-3}$ | 2.949 | 2.739 | 3.234 | 2.435 |
| $\mu$, mm$^{-1}$ | 4.364 | 4.370 | 11.461 | 4.837 |
| *T*, K | 90 | 90 | 90 | 90 |
| *λ*, Å | 0.710 73 | 0.710 73 | 0.710 73 | 0.710 73 |
| R1[a] | 0.0374 | 0.0186 | 0.0533 | 0.0295 |
| wR2[b] | 0.0921 | **0.0426** | **0.1411** | **0.0611** |

| param | **9** | **10** |
|---|---|---|
| empirical formula | $C_{10}H_{10}Cd_3N_{16}O_5$ | $C_8H_{12}Cd_8N_{12}O_{23}S_5$ |
| fw | 771.54 | 1703.80 |
| cryst syst | monoclinic | monoclinic |
| space group | $C2/c$ | $P2_1$ |
| *a*, Å | 19.6945(9) | 9.1409(4) |
| *b*, Å | 17.3497(8) | 13.5467(7) |
| *c*, Å | 13.8790(7) | 13.5525(7) |
| α, deg | 90 | 90 |
| *β*, deg | 91.047(2) | 108.4870(10) |
| *γ*, deg | 90 | 90 |
| *V*, Å$^3$ | 4741.6(5) | 1591.59(14) |
| *Z* | 8 | 2 |
| $D_{calcd}$, g cm$^{-3}$ | 2.162 | 3.555 |
| $\mu$, mm$^{-1}$ | 2.723 | 5.678 |
| *T*, K | 90 | 90 |
| *λ*, Å | 0.710 73 | 0.710 73 |
| R1[a] | 0.0421 | 0.0164 |
| wR2[b] | 0.1079 | 0.0371 |

[a] $R1 = \Sigma||F_o| - |F_c||/\Sigma|F_o|$. [b] $wR2 = \{\Sigma[w(F_o^2 - F_c^2)^2]/\Sigma[w(F_o^2)^2]^{1/2}\}$; $w = 1/[\sigma^2(F_o^2) + (aP)^2 + bP]$, with $P = [\max(F_o^2,0) + 2F_c^2]/3$ for all data.

600−650 cm$^{-1}$ range. The nitrate material **9** shows $\nu$(N−O) stretches at 1502 and 1153 cm$^{-1}$.

**X-ray Crystal Structures.** Triazole and its derivatives have been demonstrated to provide a wealth of coordination polymers with complex and unusual architectures and a range of physical properties. As anticipated, the hydrothermal chemistry of 1,2,4-triazolate with Zn(II) and Cd(II) is characterized by an unusually varied structural chemistry.

As shown in Figure 1b, the structure of the binary composition $[Zn(trz)_2]$ (**1**) is three-dimensional. The Zn(II) sites are tetrahedral with $\{ZnN_4\}$ coordination through bonding to two N1 and two N4 sites of four triazolate ligands. The triazolate groups bridge two zinc sites, leaving the N2 position of the rings unbound.

The complex three-dimensional structure of **1** is constructed from adamantoid $\{Zn_{10}(trz)_{12}\}$ cages, shown in

**Table 2.** Summary of the Structural Characteristics of the Compounds of This Study and Related Materials

| compd | dimensionality | coord geometry[a] | M−N | M−X(X) | substructures |
|---|---|---|---|---|---|
| $[Zn(trz)_2]$ (**1**) | 3-D | tet, $\{ZnN_4\}$ | 1.972(3)−1.996(3) | | $\{Zn_{10}(trz)_{12}\}$ cages |
| $[Zn(trz)F]\cdot H_2O$ | 3-D | trig bipy, $\{ZnN_3F_2\}$ | 2.006(3)−2.027(2) | 2.054(9), av | $\{Zn(trz)F\}_n$ chains |
| [Zn(trz)Cl] | 2-D | tet, $\{ZnN_3Cl\}$ | 2.003(5)−2.006(5) | 2.214(2) | $\{Zn_2Cl_2(trz)_4\}^{2-}$ clusters and $\{Zn_4(trz)_4\}^{4+}$ rings |
| [Zn(trz)Br] (**2**) | 2-D | tet, $\{ZnN_3Br\}$ | 2.001(2)−2.006(2) | 2.3485(3) | $\{Zn_2Br_2(trz)_4\}^{2-}$ clusters and $\{Zn_4(trz)_4\}^{4+}$ rings |
| $[Zn_2(trz)_3(OH)]\cdot 3H_2O$ (**3**$\cdot 3H_2O$) | 3-D | oct, $\{ZnN_6\}$ | 2.110(3)−2.219(3) | | $\{Zn(trz)_3\}_n^{n-}$ chains |
| | | tet, $\{ZnN_3O\}$ | 1.965(3)−1.984(2) | 2.023(2) | |
| $[Zn_2(trz)(SO_4)(OH)]$ (**4**) | 3-D | oct, $\{ZnN_2O_4\}$ | 2.079(2) | 2.043(1) (OH), 2.245(2) ($SO_4$) | $\{Zn_3(\mu^3\text{-OH})\}^{5+}$ clusters and $\{Zn_2(SO_4)(OH)\}_n^{n-}$ layers |
| $[Cd_3(trz)_3F_2(H_2O)]\cdot 2.75H_2O$ (**5**$\cdot 2.75H_2O$) | 3-D | oct, $\{CdN_3F_3\}$ | 2.252(5)−2.271(5) | 2.289(3)−2.421(3) (F), 2.238(9) ($H_2O$) | $\{Cd_4F_4\}^{4+}$ clusters, $\{Cd_6(trz)_6F_4(H_2O)_2\}^{2+}$ clusters |
| | | trig bipy, $\{CdN_3FO\}$ | 2.259(5)−2.273(5) | | $\{Cd_6(trz)_6F_4(H_2O)_2\}_n^{2n+}$ chains |
| $[Cd_2(trz)_2Cl_2(H_2O)]$ (**6**) | 3-D | oct, $\{CdN_4Cl_2\}$ and $\{CdN_2Cl_3O\}$ | 2.303(2)−2.306(2), 2.217(2) | 2.303(2)−2.306(2) (Cl), 2.7097(8)−2.7406(8) (Cl) | $\{Cd(trz)_2Cl\}_n^{n-}$ chains, $\{Cd(trz)_2Cl_2(H_2O)\}_n^{2n-}$ chains |
| $[Cd_3(trz)_3Br_3]$ (**7**) | 3-D | oct, $\{CdN_2Br_4\}$ and $\{CdN_3Br_3\}$; trig bipy, $\{CuN_4Br\}$ | 2.194(8)−2.201(9), 2.279(9)−2.319(9); 2.226(9)−2.313(9) | 2.798(1)−2.972(1), 2.724(1)−2.981(1); 2.668(1) | $\{Cd(trz)_2Br_2\}_n^{2n-}$ chains, $\{Cd_3(trz)_2Br_3\}_n^{n+}$ layers |
| $[Cd_2(trz)_3I\}]$ (**8**) | 3-D | oct, $\{CdN_6\}$; tet, $\{CdN_3O\}$ | 2.296(5)−2.411(5); 2.189(5)−2.210(3) | -; 2.7469(6) | $\{Cd(trz)I\}$ chains |
| $[Cd_3(trz)_5(NO_3)(H_2O)]\cdot H_2O$ (**9**$\cdot H_2O$) | 3-D | oct, $\{CdN_6\}$; 2 × trig bipy, $\{CdN_3O_2\}$ and $\{CdN_4O\}$ | 2.315(5)−2.374(4); 2.203(5)−2.256(7), 2.210(5)−2.337(1) | -; 2.493(5) ($NO_3$), 2.531(5) ($H_2O$) | $\{Cd(trz)_3\}_n^{n-}$ chains, $\{Cd_2(trz)_7(H_2O)_2\}^{3-}$ clusters |
| $[Cd_8(trz)_4(OH)_2(SO_4)_5(H_2O)]$ (**10**) | 3-D | oct, $\{CdN_2O_4\}$ (×4) | 2.186(3)−2.338(3) | 2.186(2)−2.320(2) (OH) | $\{Cd_3(\mu^3\text{-OH})\}^{5+}$ clusters, $\{Cd_7(trz)_4\}^{10n+}$ chains, $\{Cd_8(SO_4)_5\}_n^{6n+}$ framework |
| | | $\{CdNO_5\}$ (×1) | 2.148(2) | 2.303(2)−2.446(2) ($SO_4$) | |
| | | $\{CdNO_5\}$ (×1) | 2.239(3) | 2.288(2)−2.501(3) ($SO_4$), 2.299(3) ($H_2O$) | |
| | | $\{CdO_6\}$ (×1) | | 2.272(2)−2.362(2) ($SO_4$), 2.262(2) (OH) | |
| | | $\{CdN_2O_4\}$ (×1) | 2.207(3)−2.213(3) | 2.296(2)−2.540(3) ($SO_4$) | |

[a] Key: tet, tetrahedral; trig bipy, trigonal bipyramidal; oct, octahedral.

Figure 1c, which link to adjacent cages through the zinc nodes. The volume of the cage pore of ca. 1500 Å allows interpenetration of the three-dimensional framework by a second, independent three-dimensional unit. The observation of such inextricably interpenetrated framework structures is not unusual in the structural chemistry of metal−organic frameworks.

The bromide phase [Zn(trz)Br] (**2**) is the only two-dimensional structure of this study (Figure 2b). The network is constructed from tetrahedral $\{ZnN_3Br\}$ sites, with the coordination geometry at each zinc site defined by nitrogen donors from three triazolates and a terminal bromine ligand. The secondary building unit is a binuclear $\{Zn_2Br_2(trz)_4\}^{2-}$ cluster, with zinc centers bridged by two triazolates in the N1,N2-bridging mode, to form a $\{Zn_2N_4\}$ heterocycle. Each zinc atom also bonds to the N4 position of an exocyclic triazolate ligand. The binuclear units are interlinked through the remaining sites of the triazolate groups. This connectivity pattern generates a second ring structure $\{Zn_4(NCN)_4\}$. As shown in Figure 2b, the bromine atoms project from either face of the layer and interdigitate with the bromine atoms from adjacent layers.

The structure of **2** is quite distinct from that of the previously reported zinc(II)/triazolate/fluoride phase. The open-framework, three-dimensional structure of $[Zn(trz)F]\cdot H_2O$ is illustrated in Figure 3a. The building blocks of the structure are chains of trigonal bipyramidal Zn(II) centers with $\{ZnN_3F_2\}$ coordination, running parallel to the crystallographic *c*-axis. The coordination geometry at the zinc sites is defined by three nitrogen donors from three triazolate ligands in the equatorial plane and two axial fluoride ligands.

The chain substructure reveals zinc centers bridged by two fluoride ligands and triazolate ligands in the N1,N2-bridging mode (Figure 3b). In addition, each zinc is coordinated to the N4 position of a third triazolate. The chains are in turn interconnected through the remaining triazolate nitrogen donors into the framework structure of Figure 3a. When observed along the *c*-axis direction, it is evident that alternate triazolate groups project at angles of 120° to produce the hexagonal grid pattern for the framework, shown in Figure 3a. The framework hexagon is approximately 8 Å on an edge, resulting in a "free" volume of 43.9%. The channels are occupied by the water of crystallization. However, the zinc chloride phase [Zn(trz)Cl] exhibits the same corrugated layer structure as **2** and is isomorphous with **2**.

The three-dimensional structure of $[Zn_2(trz)_3(OH)]\cdot 3H_2O$ (**3**$\cdot 3H_2O$) is shown in Figure 4b. The structure is best described as $\{Zn(trz)_3\}_n^{n-}$ chains, running parallel to the *a*-axis, linked through tetrahedral $\{ZnN_3(OH)\}$ sites. As shown in Figure 4c, the chain is constructed from octahedral $\{ZnN_6\}$ centers. Each zinc site is bridged to each of two adjacent zinc sites through three triazolate ligands in the N1,N2-bridging mode. Consequently, the triazolate groups project outward from the Zn···Zn axis of a chain so as to make an angle of 60° between the planes of alternate triazolate rings when the chain is projected onto the *bc*-plane.

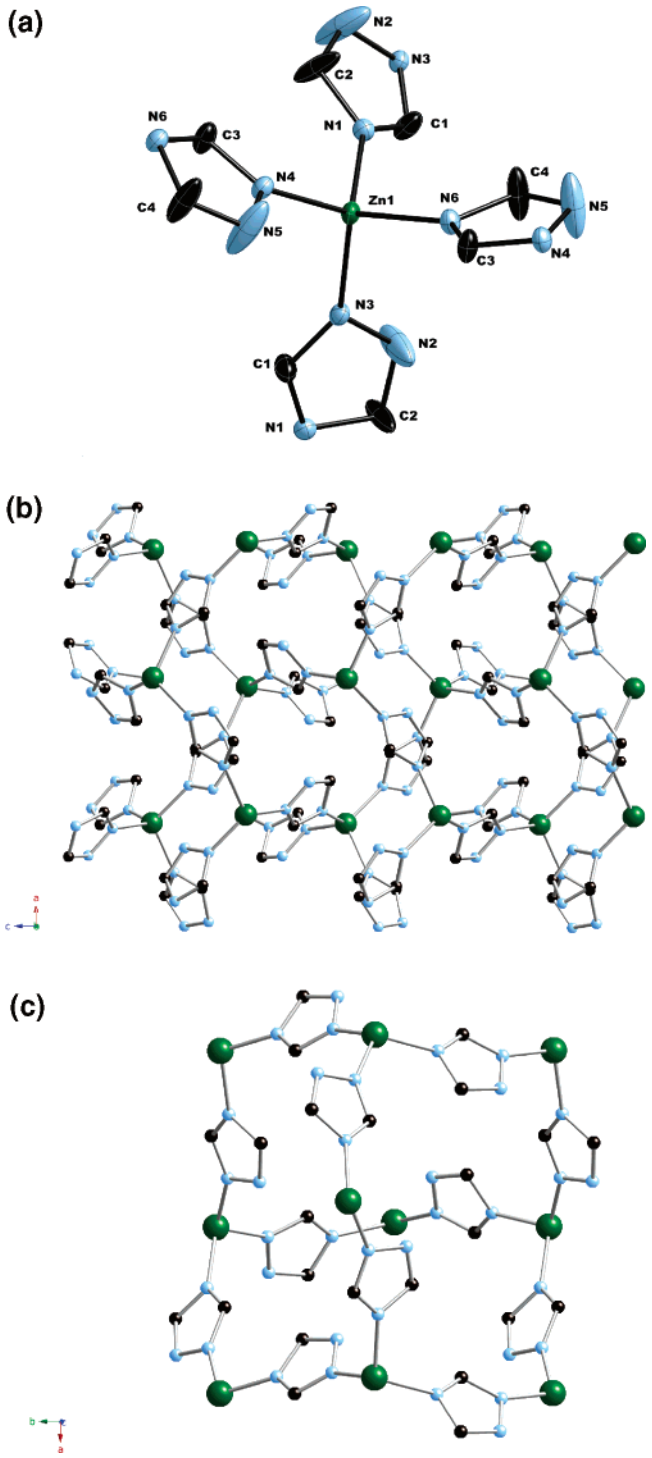


**Figure 1.** (a) View of the structure of $[Zn(trz)_2]$ (**1**), showing the atom-labeling scheme and 50% thermal ellipsoids. (b) View of the three-dimensional structure of **1** in the *ac*-plane. (c) Adamantoid $\{Zn_{10}(trz)_{12}\}$ cage that provides the secondary building unit for **1**.

The N4 position of each triazolate ligand bonds to the tetrahedral zinc sites, each of which bridges to three adjacent $\{Zn(trz)_3\}_n^{n-}$ chains through the three triazolate groups. The coordination geometry at this second zinc site is completed by a hydroxy group. The connectivity pattern generates the centered hexagonal network in projection onto the *b*c-plane, as illustrated in Figure 4b. The water molecules of crystallization occupy the volume between chains, both the

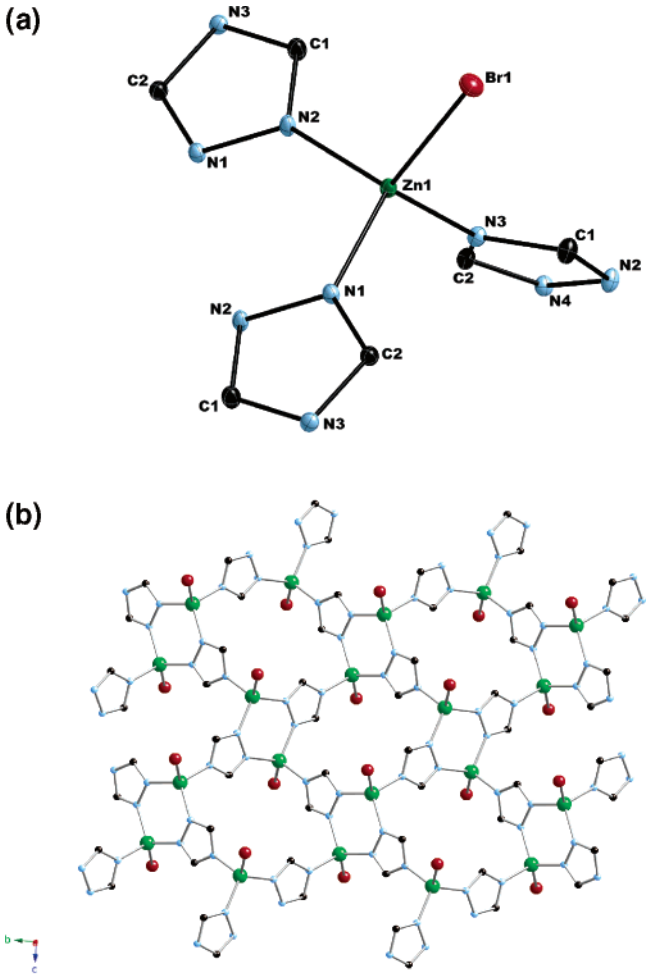


**Figure 2.** (a) ORTEP view of the structure of [Zn(trz)Br] (**2**), showing the atom-labeling scheme and 50% thermal ellipsoids. (b) Ball and stick representation of the two-dimensional structure of **2** in the *bc*-plane.

rhomboid void channels and the regions above and below the $\{ZnN_3(OH)\}$ sites.

The sulfate phase $[Zn_2(trz)(SO_4)(OH)]$ (**4**) also manifests a complex three-dimensional structure, shown in Figure 5b. The structure may be described as $\{Zn_2(SO_4)(OH)\}_n^{n-}$ layers in the *ab* plane, shown in Figure 5c, linked in the third dimension through triazolate ligands. As shown in Figure 5b, the stacking of Zn/S/O layers produces interlamellar regions populated by the triazolate ligands.

The secondary building units of the structure are trinuclear $\{Zn_3(\mu_3\text{-}OH)\}^{5+}$ clusters, which exhibit two distinct Zn(II) coordination geometries. The first is a distorted octahedral $\{ZnN_2O_4\}$ site, exhibited by two zinc centers of the triad. The coordination geometry is defined by N1(N2) nitrogen donors from two triazolate ligands, the $\mu_3$-hydroxy group, and an oxygen donor from each of three sulfate groups. These six coordinate zinc atoms form a chain substructure linked through N1,N2-bridging triazolate ligands and bridging hydroxy groups, running parallel to the *b*-axis.

The second zinc site exhibits distorted square pyramidal geometry with the basal plane occupied by a triazolate N4 nitrogen, two sulfate oxygen atoms and the hydroxy group, and a sulfate oxygen donor in the apical position. The $\{Zn_3(OH)\}^{5+}$ clusters form hydroxy-, triazolate-, and sulfate-

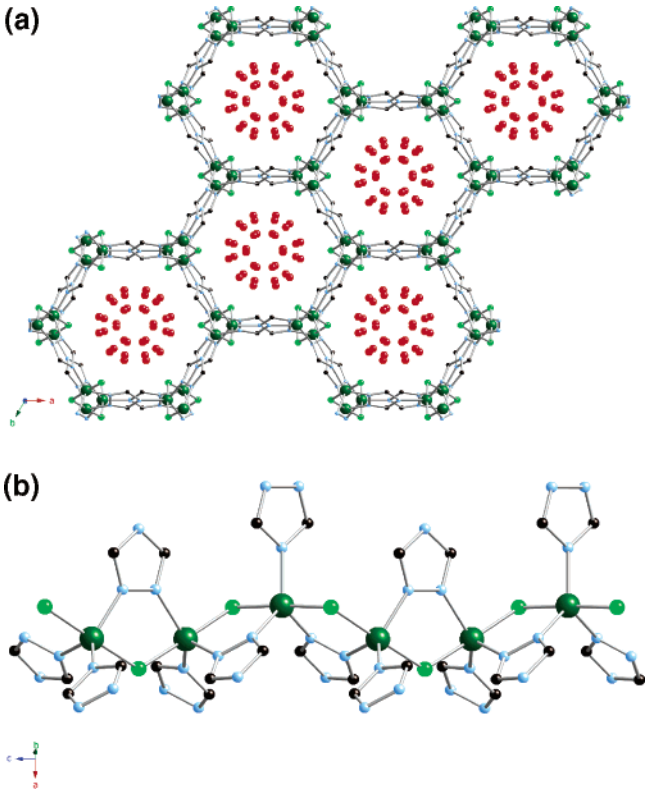


**Figure 3.** (a) View of the structure of $[Zn(trz)F]\cdot 1.33H_2O$ in the *ab*-plane, showing the large channels that contain the water of crystallization. (b) {Cd(trz)F} chain substructure of $[Zn(trz)F]\cdot 1.33H_2O$.

bridged chains in the *ab*-plane. The chains are in turn connected into a network through bridging sulfate groups. Each sulfate adopts a $\eta^3$, $\mu_5$ coordination mode, using three oxygen donors and leaving a single pendant {S−O} group on each sulfate site. The sulfate moieties bridge two octahedral and two square pyramidal zinc sites of a chain and bridge to a square pyramidal zinc of an adjacent chain to produce the layer substructure of Figure 5c. The layers stack along the *c*-direction. Each triazolate ligand adopts the N1,N2,N4-bridging mode, linking two six coordinate zinc sites of the chain and a square pyramidal zinc of an adjacent layer.

The cadmium fluoride phase $[Cd_3(trz)_3F_2(OH)]\cdot 3H_2O$ (**5**·$3H_2O$) adopts the three-dimensional structure of Figure 6b. There are two distinct cadmium sites: six coordinate $\{CdN_3F_3\}$ centers defined by three triazolate nitrogens, two $\mu_3$-fluoride ligands, and a $\mu_4$-fluoride and a distorted trigonal bipyramidal $\{CdN_3FO\}$ site defined by three triazolate nitrogen donors, a $\mu_4$-fluoride, and a hydroxo ligand.

The secondary building unit is a hexanuclear cadmium cluster, shown in Figure 6c. The cluster consists of a central $\{Cd_4F_4\}$ core of six coordinate cadmium centers. The core is linked to two five-coordinate cadmium sites through the $\mu_4$-fluoride donors and through N1,N2-bridging triazolate groups. Each of two cadmium centers of the central core participates in two N1,N2-bridging interactions with a five-coordinate site, while the remaining two cadmium atoms of the core participate in a single triazolate bridge with the five coordinate sites. Consequently, two cadmium centers of the core participate in two N1(N2) interactions

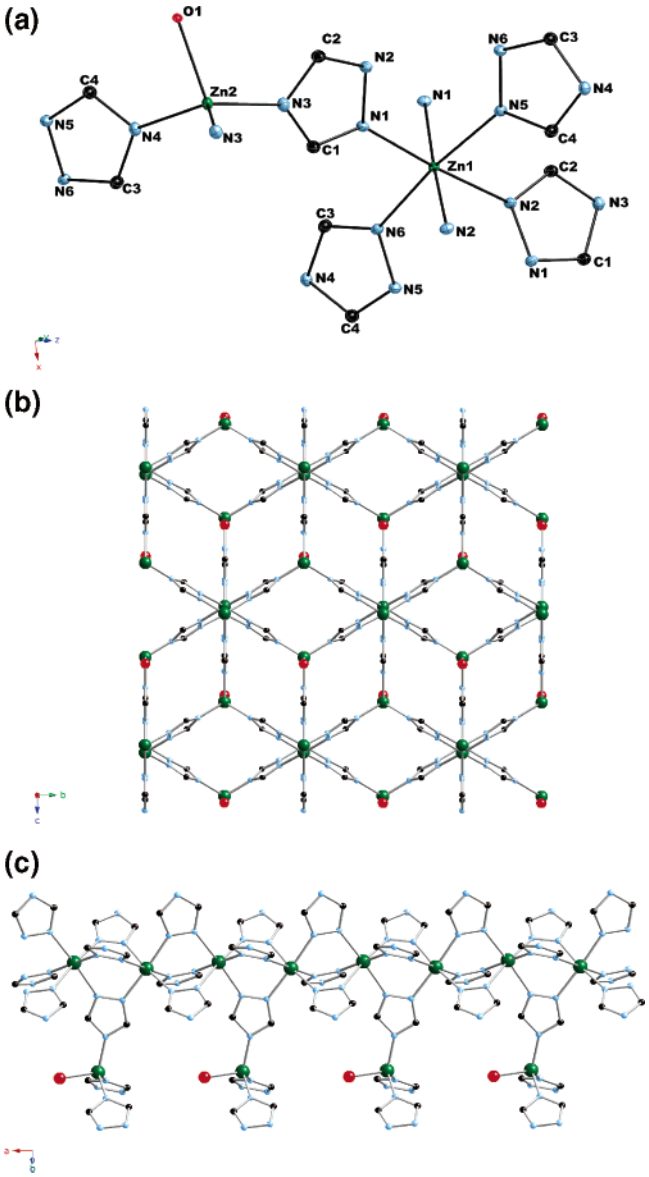


**Figure 4.** (a) Atom-labeling scheme and 50% thermal ellipsoids for the structure of $[Zn_2(trz)_3(OH)]\cdot 3H_2O$ (**3**·$3H_2O$). (b) View of the three-dimensional structure of **3**. (c) $\{Zn(trz)_3\}_n^{n-}$ chain and one set of the tetrahedral zinc sites that serve to link adjacent chains.

and a single N4 bond to an exo-core triazolate, and the remaining two metal centers exhibit a single N1(N2) bridge and two bonds to N4 sites of exo-cluster triazolate groups. These clusters are linked through triazolate nitrogen donors into chains, running parallel to the crystallographic *a*-axis (Figure 6d).

The connectivity pattern generates intersecting hydrophilic channels parallel to the *a*- and *c*-axes. The aqua ligands project into these channels which are also occupied by the water molecules of crystallization.

Multiple coordination modes are also observed for $[Cd_2(trz)_2Cl_2(H_2O)]$ (**6**), whose three-dimensional structure is depicted in Figure 7b. The complex structure may be understood in terms of two one-dimensional substructures. The first is a chain of distorted six coordinate $\{CdN_4Cl_2\}$ sites. Each cadmium site of this chain is linked to two adjacent sites through two N1,N2-bridging triazolate ligands and a bridging

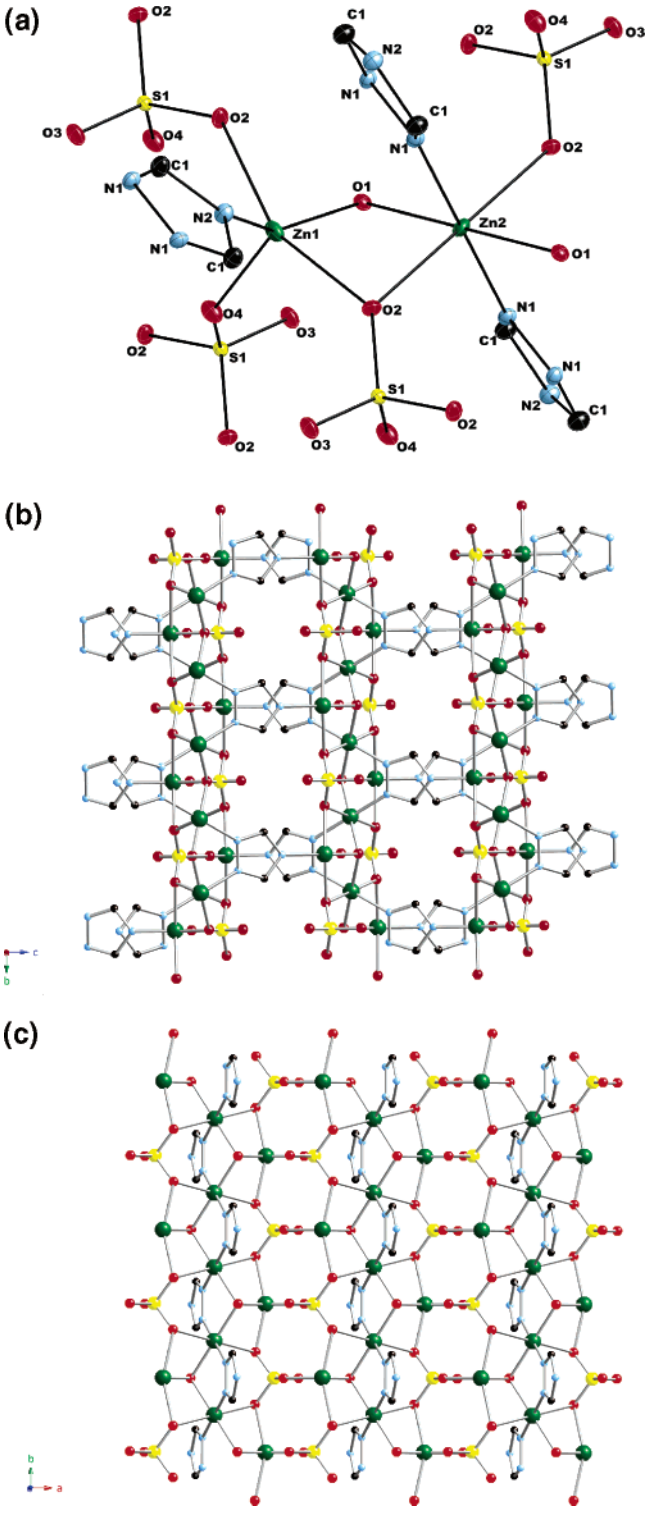


**Figure 5.** (a) ORTEP view of the atom-labeling scheme and 50% thermal ellipsoids for $[Zn_2(trz)(SO_4)(OH)]$ (**4**). (b) View of the three-dimensional structure of **4**. (c) Layer substructure of **4** in the *ab*-plane.

chloride to each neighbor. The transoid disposition of the chloride donors produces a zigzag $\{CdCl\}_n$ core.

The second cadmium coordination geometry $\{CdN_2Cl_3O\}$ participates in a second chain substructure that propagates parallel to the first chain in the *ac*-plane (Figure 7c). Each cadmium of this type bonds to two N4-triazolate nitrogen donors in a transoid disposition, two cisoid $\mu_2$-Cl donors that bridge exclusively to cadmium sites of this chain, an aqua ligand, and a $\mu_3$-chloride donor that serves to link the two types of chain in the *ac*-plane. Propagation into the third dimension is achieved through the triazolate nitrogen donors that are not involved in bonding to cadmium sites in the plane of Figure 7c. Alternatively, the structure could be described as $\{CdCl\}_n^{n+}$ layers, parallel to the *ac* plane, linked through triazolate ligands into a framework structure. This description is revealed in Figure 7b.

A view of the three-dimensional structure of $[Cd_3(trz)_3Br_3]$ (**7**), projected onto the *ab*-plane, is shown in Figure 8b. While the connectivity pattern for **8** is unusually complex and based on the presence of three distinct cadmium polyhedra, $\{CdN_2Br_4\}$, $\{CdN_3Br_3\}$, and $\{CdN_4Br\}$, the structure may be described most simply as Cd/Br/triazolate layers parallel to the *ac*-plane, linked through additional triazolate ligands in the third dimension. A view of the layer substructure of **7**, shown in Figure 8c, illustrates the structural complexity deriving from the three cadmium environments. The $\{CdN_2Br_4\}$ octahedra (type 1) are defined by four bromine donors in the equatorial plane and two triazolate nitrogen donors in the axial positions. These octahedra engage in opposite edge-sharing through the bromine ligands to generate $\{CdBr_2\}_n$ chains, parallel to the *c*-axis. This chain is decorated with $\{CuN_3Br_3\}$ sites (type 2), alternating at either edge of the chain. These second cadmium sites participate in bonding to $\mu_3$-bromine atoms of the chain and are additionally linked to the chain cadmium sites through an N1,N2-triazolate bridge. Thus, the$\{CuN_3Br_3\}$ centers exploit their remaining bromine and triazolate groups to bridge to three Cd sites of the third type $\{CdN_4Br\}$. Type 2 cadmium bridges to one type 3 site through a $\mu_2$-bromine and an N1,N2-triazolate linkage. In addition, the type 2 sites bond to the N4 donor of a triazolate group which uses the remaining N1,N2 positions to bridge two additional type 3 cadmium sites. The distorted trigonal bipyramidal type 3 sites form binuclear $\{Cd_2(1,2\text{-triazolate})_2\}$ subunits, each of which bridges to four cadmium type 2 sites of the layer and four type 2 and two type 3 cadmium sites on adjacent layers. In the *ac*-plane, the type 2 and type 3 cadmium sites form a ribbon that propagates parallel to the type 1 chain. The alternating chains and ribbons connect to form the layer substructure. The triazolate groups project from either face of the layer and serve to link the layers in the *b*-direction.

The three-dimensional structure of $[Cd_2(trz)_3I]$ (**8**) is isomorphous with that of $[Zn_2(trz)_3(OH)]$ (**3**). As shown in Figure 9, compound **8** exhibits the centered hexagonal projection in the *bc*-plane. The metrical differences between **8** and **3** reflect the substitution of Cd(II) for Zn(II) and $I^-$ and $OH^-$. Despite a 14% increase in volume of **8** compared to **3**, the crystals of **8** do not contain water of crystallization.

The three-dimensional structure of $[Cd_3(trz)_5(NO_3)(H_2O)]\cdot H_2O$ (**9**·$H_2O$), shown in Figure 10b, is constructed from the $\{M(II)(trz)_3\}_n^{n-}$ chains, previously described for compounds **3** and **8**. However, the connectivity between chains in **9** is provided by two unique structural elements, as shown in Figure 10c, providing an architecture constructed from three distinct cadmium coordination polyhedra. The first are the $\{CdN_6\}$ sites of the $\{Cd(trz)_3\}_n^{n-}$ chains. These chains are

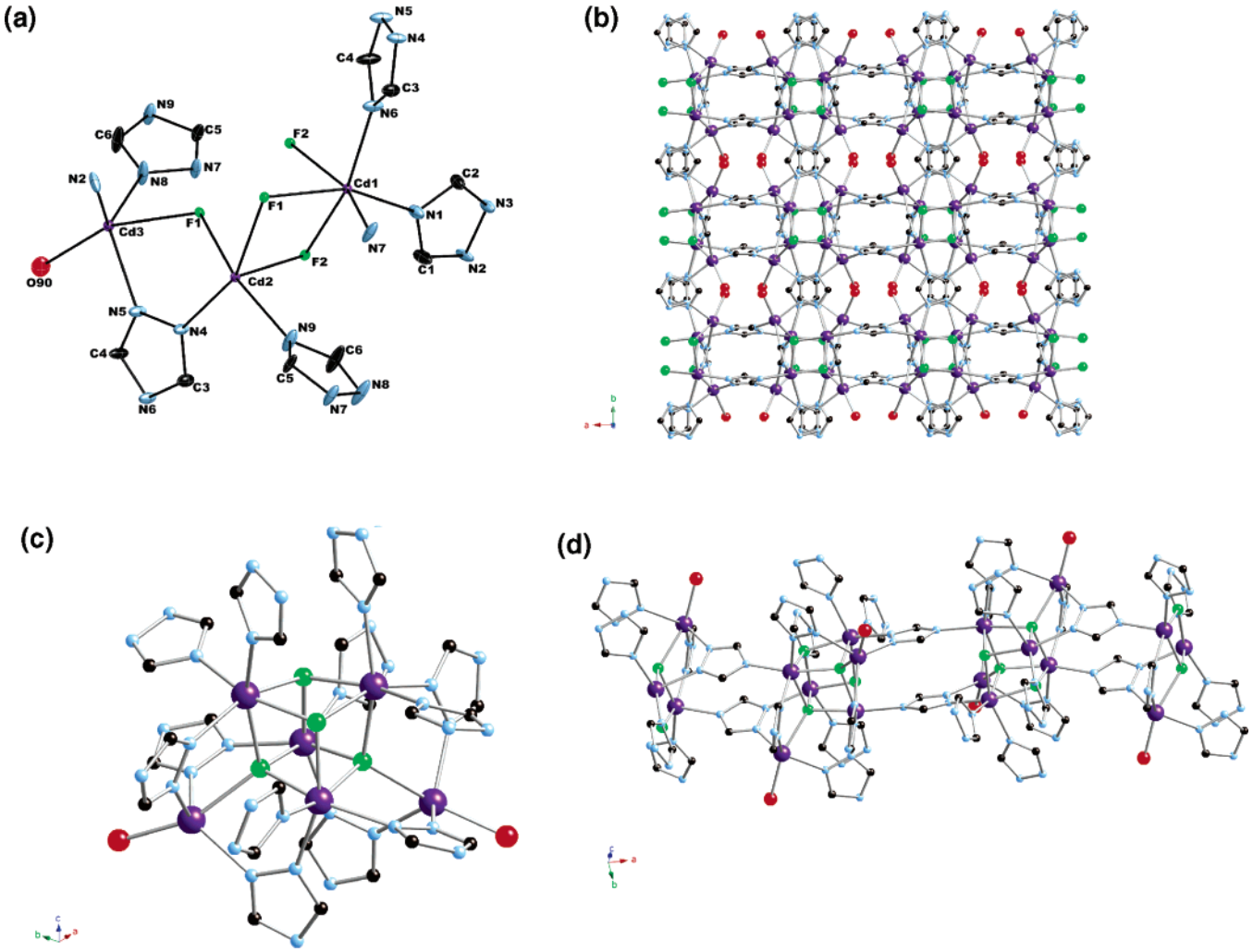


**Figure 6.** (a) View of the structure of $[Cd_3(trz)_3F_2(OH)]\cdot 3H_2O$ (**5**·$3H_2O$), showing the atom-labeling scheme and 50% thermal ellipsoids. (b) View of the three-dimensional structure of **5** in the *ab*-plane. (c) Hexanuclear cadmium building block of **5**, showing the $\{Cd_4F_4\}$ core. (d) Chain of hexanuclear clusters linked through triazolate bridges.

analogous to the $\{Zn(trz)_3\}_n^{n-}$ chains of **3** and exhibit the same profile with triazolate rings at 60° angles with respect to each other about the chain axis. The remaining structural components are the trigonal bipyramidal $\{CdN_3O_2\}$ sites and binuclear $\{Cd_2(trz)_7(H_2O)_2\}^{3-}$ sites which connect a given chain to six neighboring chains.

The first five coordinate cadmium site is defined by three N4 triazolate donors in the equatorial plane and two axial sulfate oxygen donors. The sulfate ligands are monodentate with the uncoordinated oxygen atoms aligned parallel to the *b*-axis. The triazolate ligand planes of this cadmium site are disposed at ca. 120° to each other and parallel to the axes of the $\{Cd(trz)_3\}_n^{n-}$ chains. Three adjacent $\{Cd(trz)_3\}_n^{n-}$ chains are linked through these five coordinate cadmium sites.

The cadmium atoms of the binuclear $\{Cd_2(trz)_7\}^{3-}$ clusters exhibit distorted $\{CdNO_4\}$ trigonal bipyramidal geometry. Each cadmium center of the cluster coordinates to three triazolate ligands through the N4 positions. The binuclear site bridges three adjacent $\{Cd(trz)_3\}_n^{n-}$ chains through these triazolate groups. When the structure is viewed down the chain axis (Figure 10b), it is observed that the planes of the triazolate groups of the binuclear clusters align parallel to and are eclipsed by the planes of the triazolate ligands of the five-coordinate cadmium sites. The triazolate ligand bridging the two cadmium centers of this binuclear unit adopts the N1,N4-bridging mode, leaving the N2 site uncoordinated.

The connectivity pattern generates a hexagonal grid pattern in projection, similar to that previously observed for compounds **3** and **8**. However, in the latter materials, the metal site of the chain linking motif $\{Zn(trz)_3(OH)\}^{2-}$ or $\{Cd(trz)_3Br\}^{2-}$ occupies the centroid of the virtual hexagons. In the case of **9**, the Cd···Cd axes of the $\{Cd_2(trz)_7\}^{3-}$ and $\{Cd(trz)_3(SO_4)_2\}^{5-}$ subunits are displaced ca. 0.4 Å from the centroids of the hexagons. Consequently, for compounds **3** and **8**, the projected hexagons are divided by the $\{Zn(trz)_3(OH)\}^{2-}$ and $\{Cd(trz)_3Br\}^{2-}$ subunits into three equivalent rhombs with edge dimensions of 6.2 and 6.4 Å, respectively. In contrast, the $SO_4^{2-}$ groups of adjacent virtual chains of $\{Cd(trz)_3(SO_4)_2\}^{5-}/\{Cd_2(trz)_7\}^{3-}$ chains of **9** project into one rhomb and the Cd···Cd vectors of adjacent virtual chains are displaced toward each other from the centroids of the hexagonal grid. This results in division of the hexagons into two equivalent rhombs with diagonals of 8.2 and 13.1 Å and a flattened rhomb with diagonals of 5.8 and 19.7 Å. The sulfate groups project into the latter rhomb, while the

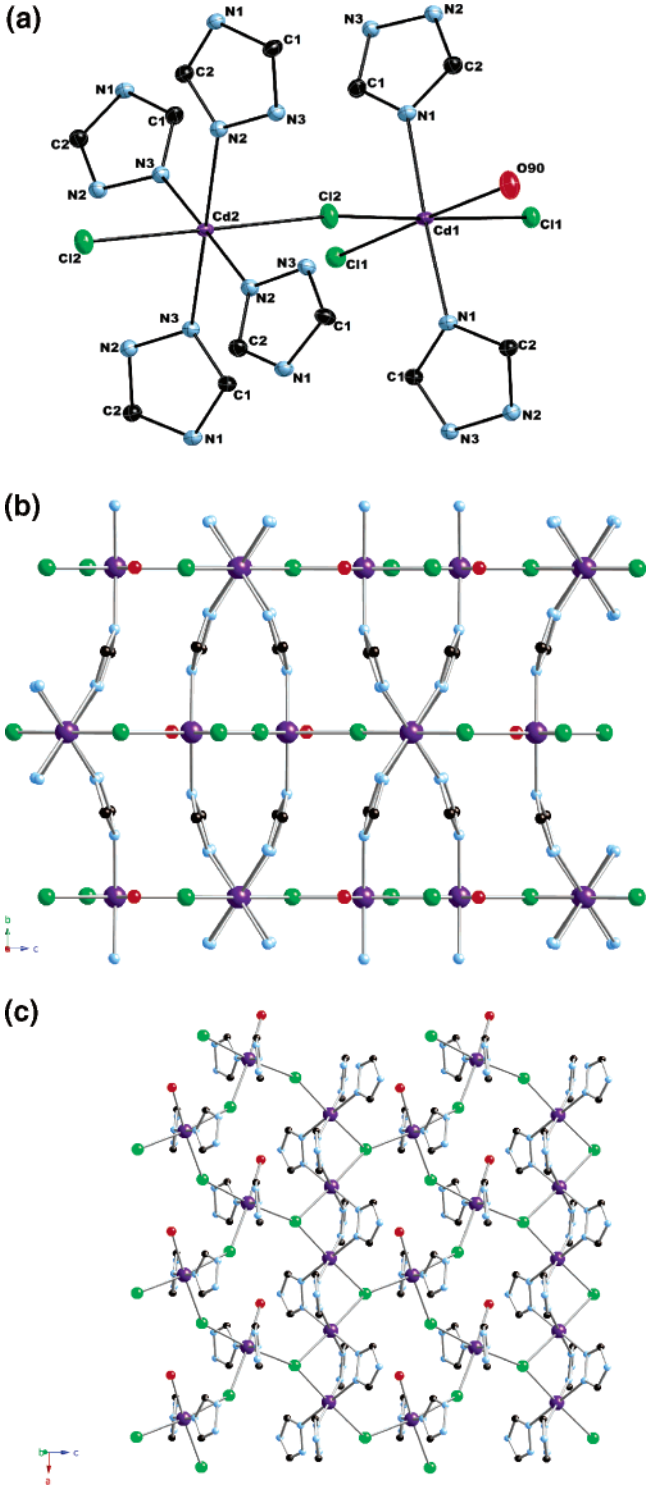


**Figure 7.** (a) Atom-labeling scheme and 50% thermal ellipsoids for the structure of $[Cd_2(trz)_2Cl_2(H_2O)]$ (**6**). (b) View of the three-dimensional structure of **6** in the *bc*-plane. (c) View of the structure of **6** in the *ac*-plane, showing the $\{Cd(trz)_2Cl\}_n^{n-}$ chains running parallel to the *a*-axis.

N1,N4-bridging triazolate groups of the $\{Cd_2(trz)_7\}^{3-}$ clusters project into the former. Apparently, the volume enclosed by the flattened rhombs is inaccessible to solvent, as the water of crystallization is found exclusively in the void regions defined by the former rhombs.

The complex three-dimensional structure of the cadmium−sulfate phase $[Cd_8(trz)_4(OH)_2(SO_4)_5(H_2O)]$ (**10**) is shown in

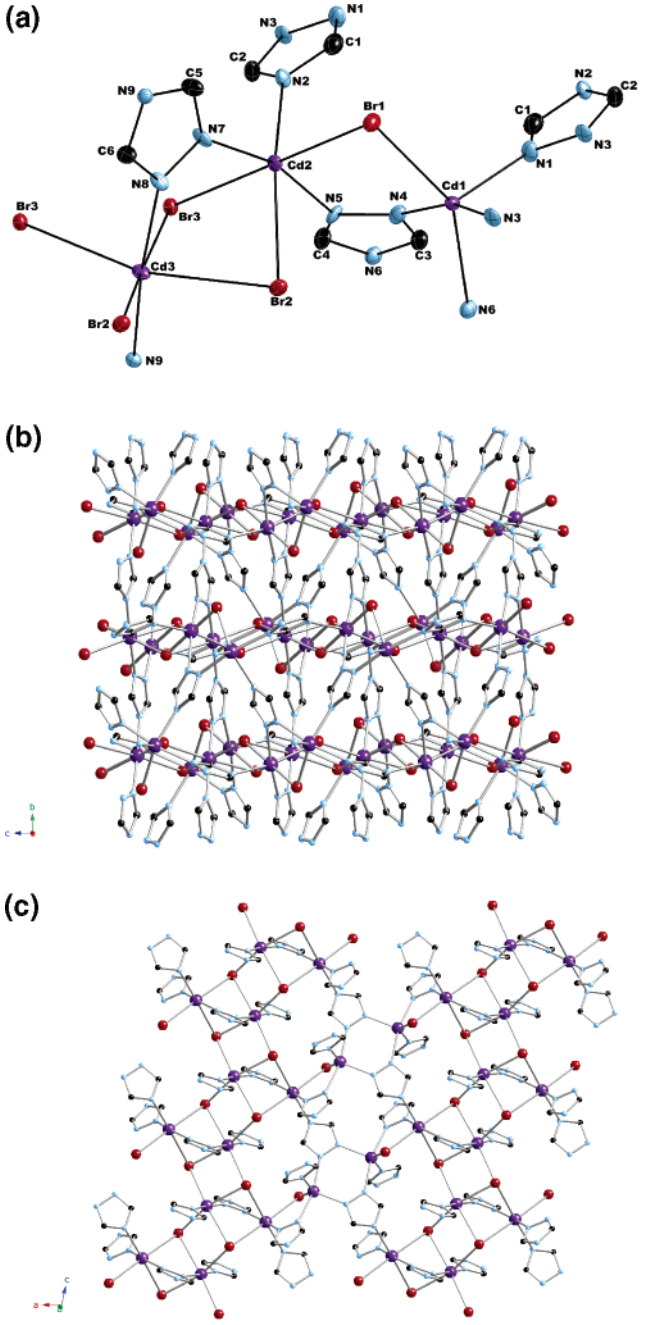


**Figure 8.** (a) ORTEP representation of the structure of $[Cd_3(trz)_3Br_3]$ (**7**), showing the atom-labeling scheme and 50% thermal ellipsoids. (b) View of the three-dimensional structure of **7** in the *bc*-plane. (c)Network substructure of **7** in the *ac*-plane showing the three cadmium environments and their linking through triazolate and bromine bridges.

Figure 11b. The structural complexity is related to the presence of eight crystallographically unique cadmium sites. Two $\{CdN_2O_4\}$ coordination sites and one $\{CdN_2O_5\}$ center form a $\mu^3$-OH-bridged triad, while a second $\mu^3$-OH-bridged triad contains two other $\{CdN_2O_4\}$ sites and a unique $\{CdO_6\}$ polyhedron, as shown in Figure 11c,d, respectively. A second $\{CdNO_5\}$ site involves aqua ligation, and there is an additional $\{CdN_2O_4\}$ site that does not participate in triad formation, illustrated in Figure 11e,f, respectively.

It is noteworthy that the cadmium sulfate substructure of **10**, $\{Cd_8(SO_4)_5\}_n^{6n+}$, is three-dimensional (Figure 11g). When projected onto the *ac*-plane, the $Cd/SO_4^{2-}$ substructure

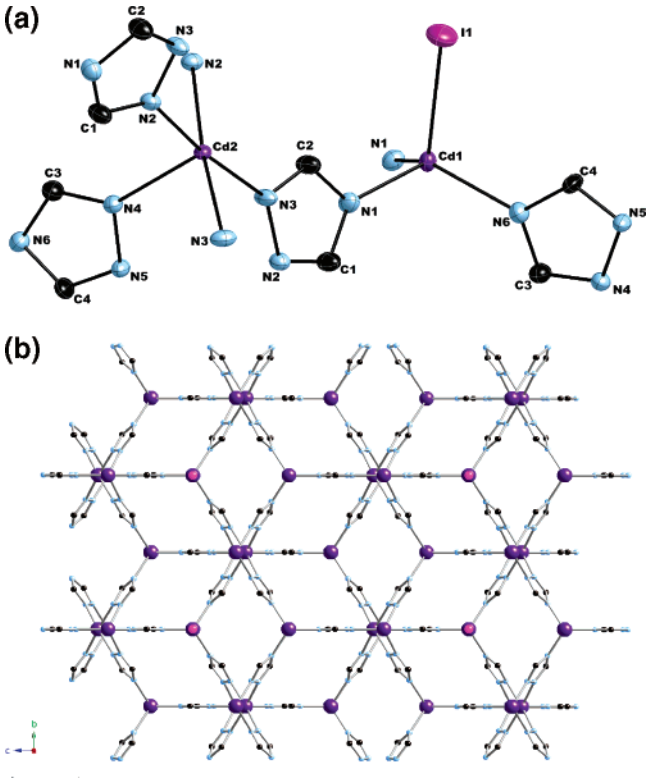


**Figure 9.** (a) View of the structure of $[Cd_2(trz)_3I]$ (**8**), showing the atom-labeling scheme and 50% thermal ellipsoids. (b) Three-dimensional structure of **8** in the *bc*-plane.

appears as cadmium sulfate layers stacking along the crystallographic *a*-axis and connected through sulfate linkages.

In contrast, the cadmium−triazolate substructure is one-dimensional, as illustrated in Figure 11h. The weaving of these strands through the three-dimensional structure of **10** is highlighted in Figure 11b. The chains propagate parallel to the *a*-axis and are constructed from $\{Cd_4(trz)_4\}^{4+}$ rings linked through exocyclic cadmium sites. The organic ligands are largely confined to the interlamellar regions between the cadmium sulfate layers of Figure 11f.

**Thermal Analyses.** The compounds of this study were analyzed by TGA under 20 mL $min^{-1}$ flowing nitrogen, while ramping the temperature at a rate of 5° $min^{-1}$ from 25 to 800 °C. The thermal decomposition profile of $[Zn(trz)_2]$ (**1**), shown in Figure 12a, is characteristic for the zinc compounds of this study, **1**−**4**. There is a rapid weight loss between ca. 375 and 450 °C attributed to the partial or total loss of the triazole components. This process is followed by a gradual weight loss in **1** and **3** from the combustion of the remaining triazole ligands. In the case of compound **4**, $[Zn_2(trz)(OH)(SO_4)]$, there is a plateau of stability between 425 and 575 °C, followed by a second sharp weight loss between 575 and 625 °C of ca. 27%, corresponding to the loss of $SO_3$ (Figure 12b).

The thermodiffraction pattern for compound **4** in the 25−450 °C temperature range is shown in Figure 13. The diffraction profile is largely unchanged to 450 °C, indicating that the zinc−oxo−sulfate framework is thermally robust and persistent to at least 450 °C. The infrared spectra of the

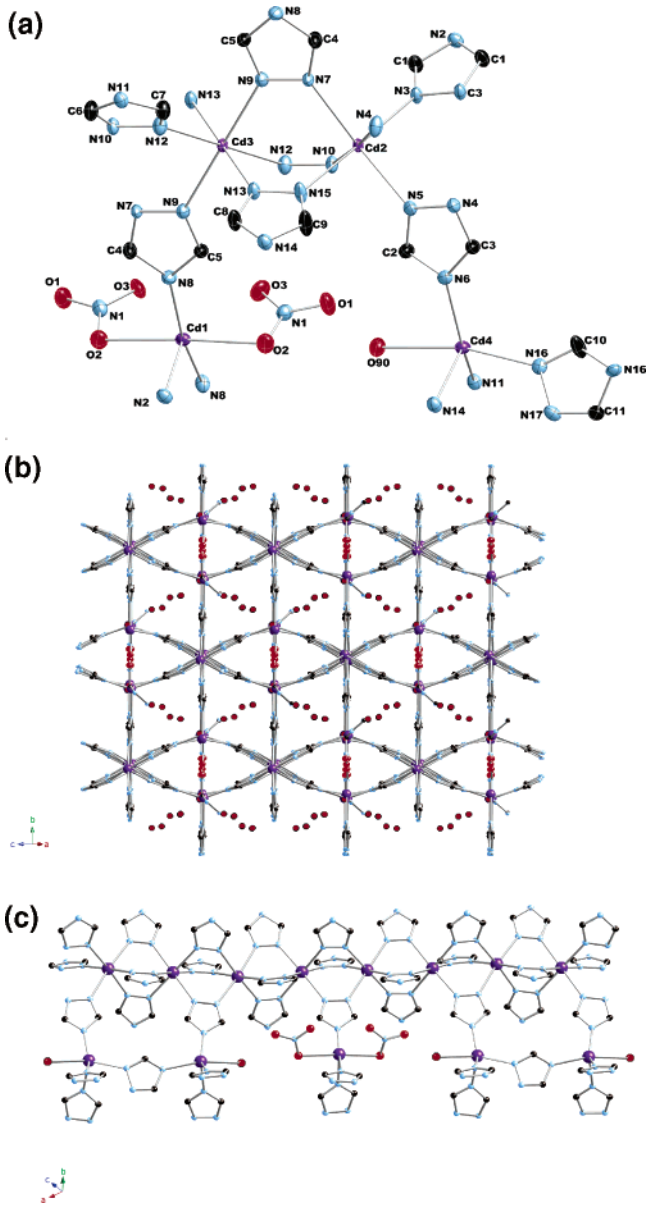


**Figure 10.** (a) ORTEP representation of the structure of $[Cd_3(trz)_5(NO_3)(H_2O)]\cdot H_2O$ (**9**·$H_2O$), showing the atom-labeling scheme and 50% thermal ellipsoids. (b) View of the three-dimensional structure of **9**. (c) $\{Cd(trz)_3\}_n^{n-}$ chain of **9** and one set of trigonal bipyramidal and binuclear $\{Cd_2(trz)_7(H_2O)_2\}^{3-}$ sites that connect the chain to neighboring chains.

products of heating to 300 and 550 °C are shown in Figure 14. The spectrum of the 300 °C product is essentially identical with that observed at room temperature. However, the spectrum of the product from heating at 550 °C is characterized by bands at ca. 2110 and 520 $cm^{-1}$, consistent with $\nu$(C≡N) and $\nu$(Zn−C) of $Zn(CN)_2$. In addition, a broad band centered at 1150 $cm^{-1}$, assigned to $\nu$(S−O) of $Zn(SO_4)$. The product of thermolysis at temperatures above 650 °C exhibits an infrared spectrum similar to that of $Zn(CN)_2$. Consequently, the thermal chemistry of **4** is consistent with the following equations:

$$[Zn_2(trz)(OH)(SO_4)] \xrightarrow{450\ ^\circ C} Zn(CN)_2 + Zn(SO_4)$$

$$Zn(CN)_2 + Zn(SO_4) \xrightarrow[650\ ^\circ C]{-SO_3} Zn(CN)_2 + ZnO$$

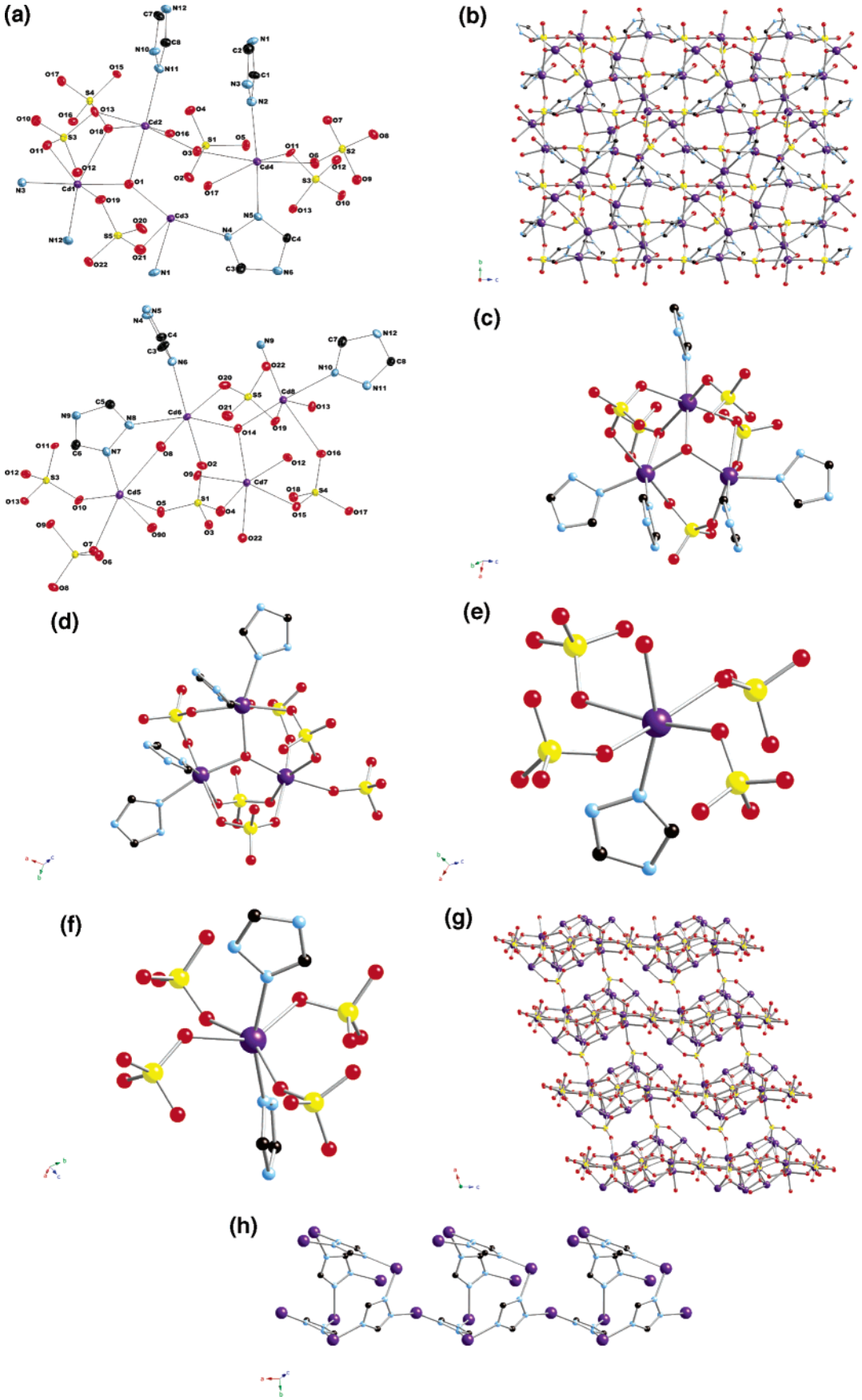


**Figure 11.** (a) Atom-labeling scheme and 50% thermal ellipsoids for the structure of $[Cd_8(trz)_4(OH)_2(SO_4)_5(H_2O)]$ (**10**). (b) View of the three-dimensional structure of **10** in the *bc*-plane. (c, d) Two $\eta^3$-OH-bridged cadmium triads that are observed as secondary building units of **10**. (e) Aqua-ligated $\{CdNO_5\}$ site of **10**. (f) "Isolated" $\{CdN_2O_4\}$ site. (g) Three-dimensional cadmium sulfate substructure of **10**. (h) One-dimensional cadmium−triazolate substructure of **10**.

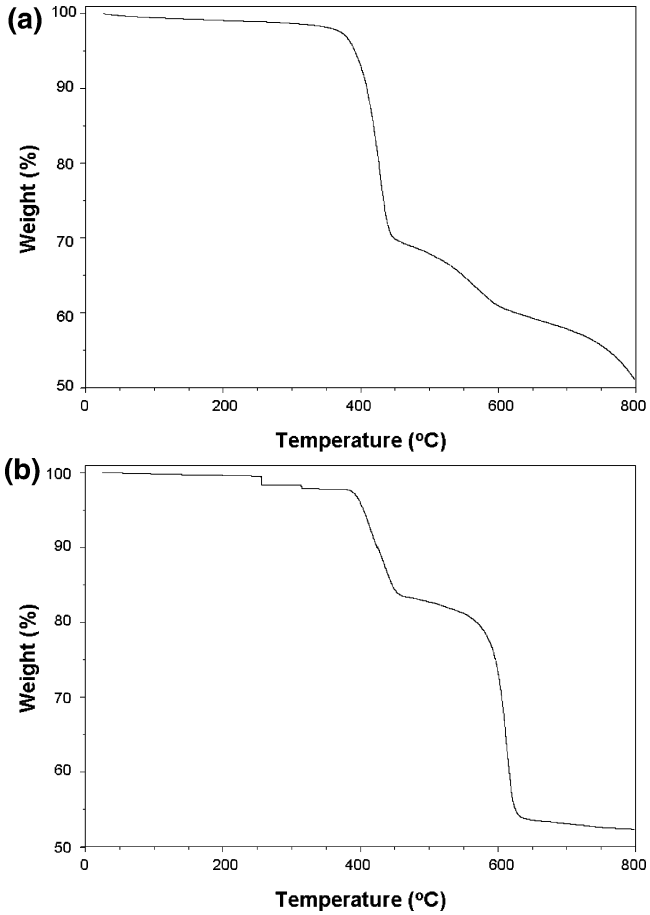


**Figure 12.** Thermogravimetric profiles in the temperature range 30−800 °C for (a) $[Zn(trz)_2]$ (**1**) and (b) $[Zn_2(trz)(OH)(SO_4)]$ (**4**).

All four zinc−triazolate phases of this study give $Zn(CN)_2$ as one product of the thermal decomposition, as monitored by infrared spectroscopy.

The cadmium series is also characterized by rapid weight loss in the 375−425 °C range, as illustrated in Figure 15a for $[Cd_3(trz)_3F_2(OH)]\cdot 3H_2O$ (**5**·$3H_2O$). In this case, there is a preliminary dehydration process between 40 and 150 °C, corresponding to the loss of the water of crystallization. The subsequent step between 370 and 390 °C, associated with the loss of the organic component, is succeeded by a plateau of stability between 400 and 600 °C. The infrared spectrum of the product of thermolysis of **5** at 550 °C exhibits bands at ca. 2200 and 675 $cm^{-1}$, consistent with the formation of $Cd(CN)_2$. Decomposition proceeds above 600 °C with sublimation of the cadmium products to complete the thermolysis. The thermodiffraction profile for compound **5** is shown in Figure 16. The pattern is generally unchanged between 25 and 450 °C, showing once more that partial loss of the organic component does not result in structural collapse. The framework of the product of the initial weight loss **5′** is thermally robust and persists to ca. 600 °C.

The cadmium bromide and cadmium iodide phases, $[Cd_3(trz)_3Br_3]$ (**7**) and $[Cd_2(trz)_3I]$ (**8**), deviate somewhat from the pattern adopted by the other members of the series. As shown in Figure 15b, compound **7** exhibits the loss of triazole in two steps between 275 and 300 °C and 410 and 430 °C. These processes are followed by loss of $Br_2$ between 450 and 550 °C and sublimation of the residual cadmium above 600 °C. The thermodiffraction pattern of **7** shows that the framework is stable to ca. 375 °C, whereupon a new crystalline phase appears (Supporting Information Figure S8).

Since $[Zn(trz)F]\cdot H_2O$ exhibits an open framework structure with considerable volume occupied by water molecules of crystallization, the thermal behavior of this material was investigated in expectation that the dehydrated [Zn(trz)F] would exhibit sorptive properties. As shown in Figure 17a, the thermogravimetric profile of $[Zn(trz)F]\cdot H_2O$ is characterized by a weight loss of ca. 10% between room temperature and 85 °C. This is followed by a plateau to 360 °C, whereupon ligand thermolysis is observed. The thermodiffraction profile for $[Zn(trz)F]\cdot H_2O$ is largely unchanged from room temperature to 450 °C, suggesting that the framework structure persists beyond the partial decomposition of the ligand above 360 °C. (Figure 17b).

**Sorptive Properties.** While the majority of the materials of this study exhibit relatively dense frameworks, several may be characterized as open three-dimensional frameworks with pores occupied by water molecules of crystallization. The most prominent of these is $[Zn(trz)F]\cdot H_2O$, whose structure reveals large, water-occupied channels running parallel to the crystallographic *c*-axis.

The material $[Zn(trz)F]\cdot H_2O$ was desolvated under dynamic vacuum at 160 °C until the outgas rate was less than 2 mTorr $min^{-1}$. The desolvated host showed $N_2$ uptake of ca. 22 mL/g when $P > 0.05$ at 77.4 K and type I absorption behavior according to the IUPAC classification (Figure 18).[85] The BET and Langmuir surface areas for [Zn(trz)F] are calculated as 66 and 108 $m^2\ g^{-1}$, respectively. The pore volume of 0.04 $cm^3\ g^{-1}$, calculated from the $N_2$ sorption data, gives a porosity of 40%, in good agreement with the estimated value of 43.9% by X-ray crystallography. The median pore width, calculated by the Horvath−Kawazoe method, is 5.3 Å.[86]

The desolvated framework also exhibits modest $H_2$ uptake with type I absorption behavior (Supporting Information Figure S9). The uptake is ca. 0.16% by weight at 150 Torr absolute pressure, with a maximum of 0.21% at 1000 Torr. The desolvated material [Zn(trz)F] also binds methanol (Figure 19), exhibiting a characteristic Langmuir isotherm. The amount of methanol absorbed at a relative pressure of 0.2 atm is ca. 6.5 wt %, rising to ca. 9.2% at 0.8 atm. The relatively modest sorption exhibited by $[Zn(trz)F]\cdot H_2O$ most likely reflects the rather narrow channel structure of the material, as well as the unidimensional nature of the channel substructure.

**Photoluminescence Properties.** Polymeric complexes of metal cations with the $d^{10}$ configuration, such as Cu(I), Zn(II), and Cd(II), and polyazaheterocyclic ligands have been shown to possess interesting luminescent properties.[61,74,87−92]

(85) IUPAC. *Pure Appl. Chem.* **1985**, *57*, 603.
(86) Horvath, G.; Kawazoe, K. *J. Chem. Eng. Jpn.* **1983**, *16*, 470.
(87) Dias, H. V. R.; Diyabalanage, H. V. K.; Eldabaja, M. G.; Elbjeirami, O.; Rawashdeh-Omary, M. A.; Omary, M. A. *J. Am. Chem. Soc.* **2005**, *127*, 7489 and references therein.
(88) Wong, W.-Y.; Liu, L.; Shi, J.-X. *Angew. Chem., Int. Ed.* **2003**, *42*, 4064.

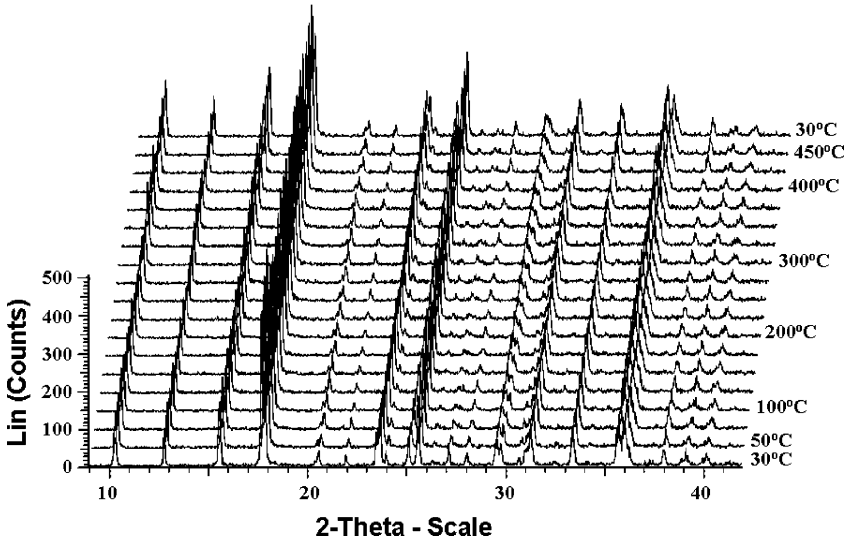


**Figure 13.** Thermodiffraction pattern of **4** in the 30−450 °C temperature range.

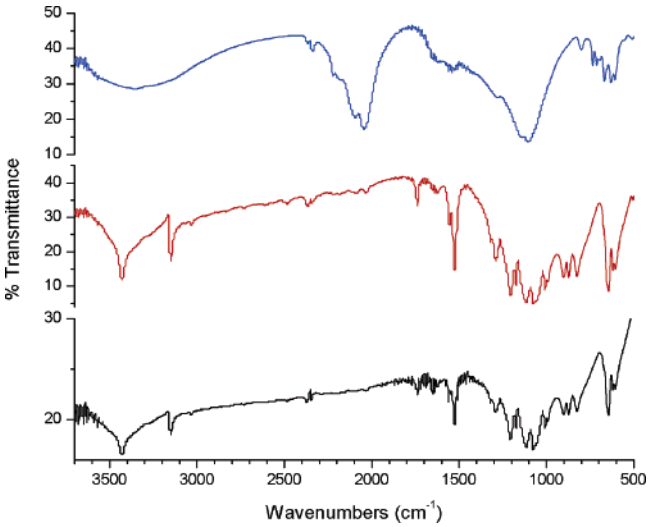


**Figure 14.** Infrared spectra of [Zn(trz)(OH)($SO_4$)] (**4**) at room temperature, 300 °C, and 550 °C.

The emissions observed for materials of the Cd(II)/4-pyridyl-1,2,4-triazole and Zn(II)/tetrazolyl classes were assigned as originating from intraligand $\pi-\pi^*$ transitions.

Sodium triazolate exhibits no observable photoluminescence, while 1,2,4-triazole itself is characterized in the solid-state spectrum at room temperature by an excitation at 318 nm, producing an emission at 421 nm (Supporting Information Figure S10). The photoluminescence of 1,2,4-triazole has been assigned as originating from $\pi-\pi^*$ transitions.

Of the materials of this study, only [Zn(trz)Cl] exhibited luminescence properties. As shown in Figure 20, excitation at 308 nm at room-temperature results in an emission at 510 nm with a lifetime of 47.2 $\mu$s. (Supporting Information Figures S11 and S12). This luminescence behavior of [Zn(trzCl)] is tentatively assigned as originating from a ligand $\pi-\pi^*$ transition. This assignment is based on the broad and unstructured emission profile, the long luminescence lifetime, and comparisons to related Zn(II) and Cd(II) solid-state materials. The photoluminescence of [Zn(trz)Cl] does not exhibit significant thermochromism.

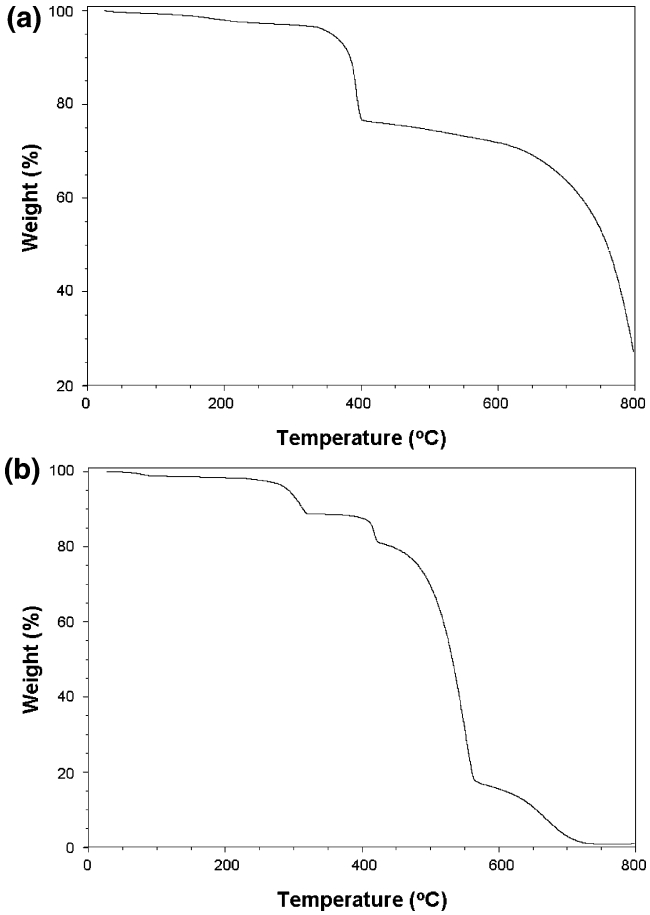


**Figure 15.** Thermogravimetric patterns in the 30−800 °C range for (a) [$Cd_3$(trz)$_3F_2$(OH)]·3$H_2O$ (**5**·3$H_2O$) and (b) [$Cd_3$(trz)$_3Br_3$] (**7**).

(89) Enomoto, M.; Kishimura, A.; Aida, T. *J. Am. Chem. Soc.* **2001**, *123*, 5608.
(90) Ding, B.; Yi, L.; Wang, Y.; Cheng, P.; Liao, D.-Z.; Yan, S.-P.; Jiang, Z.-H.; Song, H.-B.; Wang, H.-G. *Dalton Trans.* **2006**, 665.
(91) Wang, X.-S.; Tang, Y.-Z.; Huang, X.-F.; Qu, Z.-R.; Che, C.-M.; Chan, P. W. H.; Xiong, R.-G. *Inorg. Chem.* **2005**, *44*, 5278.
(92) He, X.; Lu, C.-Z.; Yuan, D.-Q. *Inorg. Chem.* **2006**, *45*, 5760.

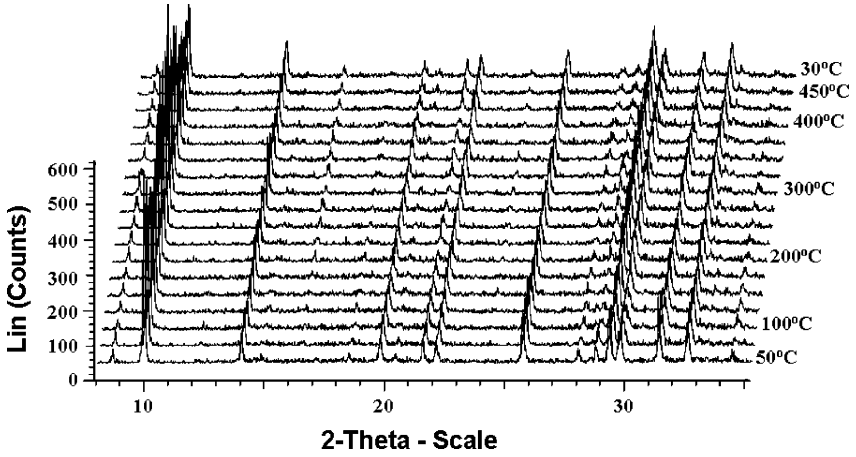


**Figure 16.** Thermodiffraction profile for compound **5** in the 30−450 °C temperature range.

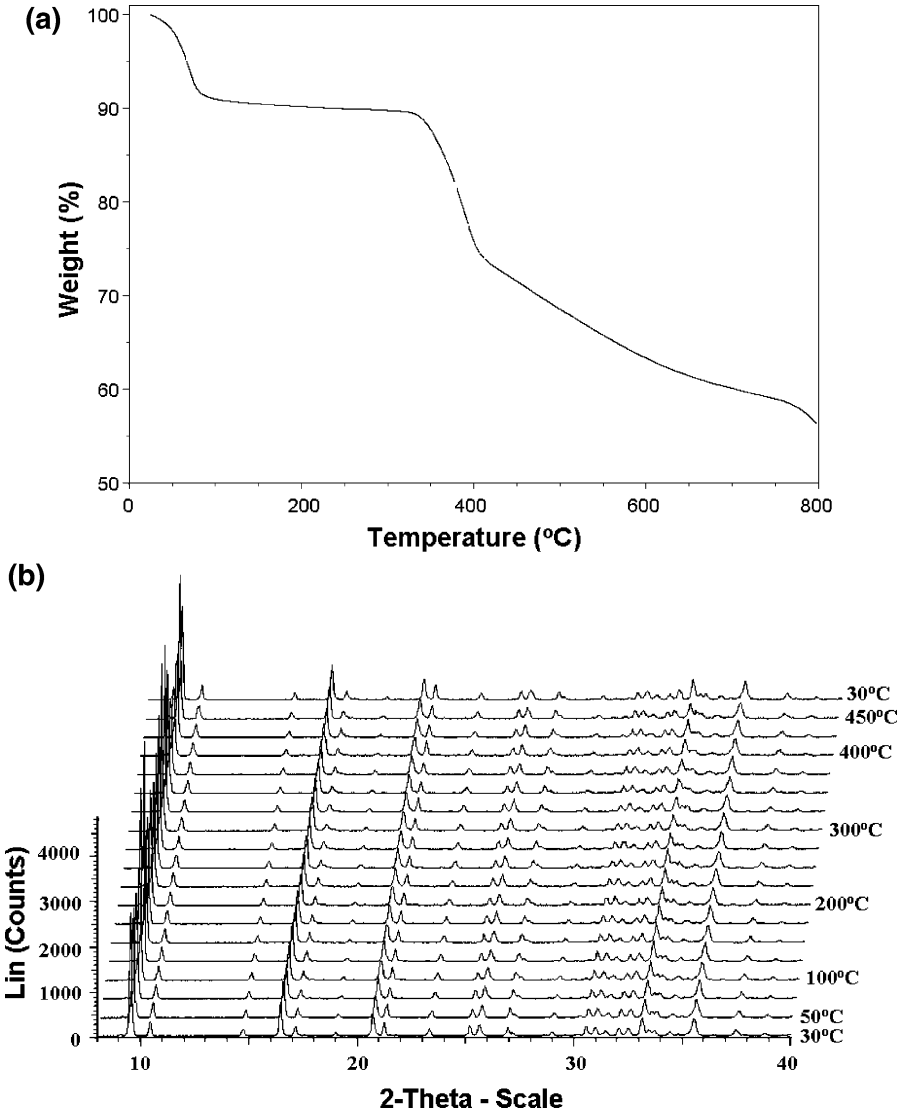


**Figure 17.** (a) Thermogravimetric profile of [Zn(trz)F]·$H_2O$ in the 30−800 °C temperature range. (b) Thermodiffraction pattern of [Zn(trz)F]·$H_2O$ in the 30−450 °C temperature range.

To understand the optical properties of [Zn(trz)Cl], solid-state density functional theory (DFT) calculations were performed. The total density of states (DOS) for [Zn(trz)Cl] is shown in Figure 21, where the partial density of states (PDOS) for the Zn 3d orbitals are shown as green curves and the ligand p-orbitals as red curves. The Fermi level is illustrated as a vertical dashed line. It is noteworthy that the calculation predicts an energy separation of 2.92 eV between the HOMO and the LUMO of [Zn(trz)Cl]. This is in good agreement with the value of 3.03 eV derived from the

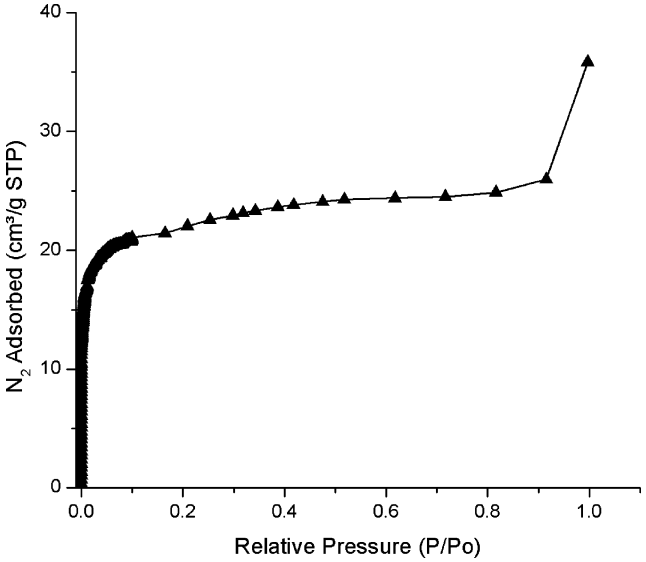


**Figure 18.** BET $N_2$ sorption isotherm for [Zn(trz)F] at 77.4 K.

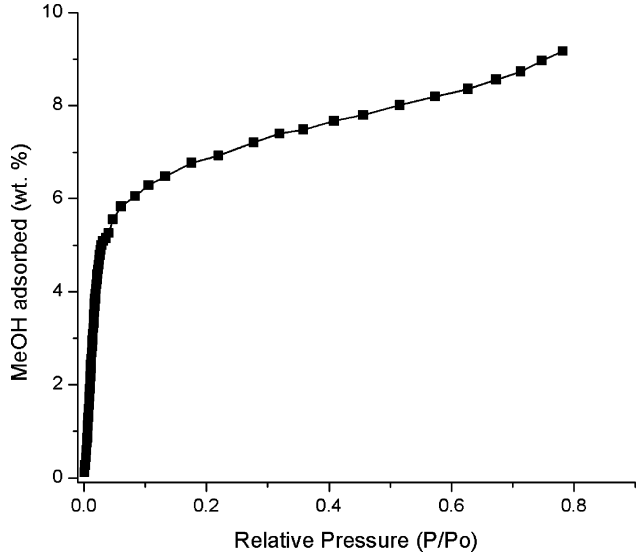


**Figure 19.** Binding of host solid [Zn(trz)F] with methanol.

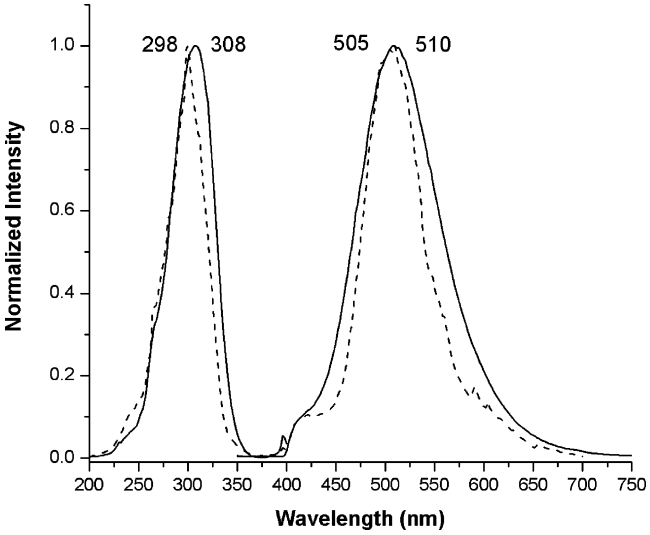


**Figure 20.** Excitation and emission spectra of [Zn(trz)Cl] at room temperature (solid lines) and 77 K (dashed lines).

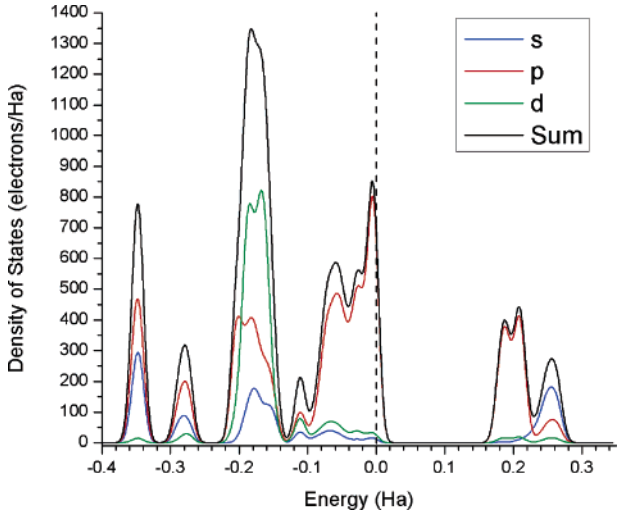


**Figure 21.** Electronic band structure of [Zn(trz)Cl]. The unit cell of [Zn(trz)Cl] contains 4 formula units.

photoluminescence spectrum for the absorption energy. The calculation also suggests that the Fermi level is largely ligand p-character and that the LUMO is dominated by ligand character.

The absence of photoluminescence for all materials of the study with the exception of [Zn(trz)Cl] was unanticipated. While any explanation of these observations remains tentative, several rationalizations present themselves. Since all the materials of the study are three-dimensional with the exceptions of the two-dimensional and isomorphous [Zn(trz)Cl] and [Zn(trz)Br], we speculate that apparently there is more vibrational coupling for the three-dimensional structures in comparison to the two-dimensional systems. Furthermore, the absence of photoluminescence for [Zn(trz)Br] suggest that the bromide analogue possesses a greater vibrational density of states which provides more effective radiationless relaxation for the bromide material than in the case of the chloride analogue.

## Conclusions

Hydrothermal methods have been exploited in the preparation of 10 materials of the M(II)−triazolate family, where M(II) is zinc or cadmium. With the exception of the homoleptic phase $[Zn(trz)_2]$ (**1**), all compounds of this study incorporated charge-balancing anions in addition to the triazolate group to provide materials of the general type M(II)/triazolate/$X^{n-}$, where $X^{n-}$ may be mononegatively changed (halide, hydroxide, or nitrate) or dinegatively charged (sulfate).

The ability of triazolate bridge to three metal centers contributes to the remarkable structural diversity of the ternary metal/triazolate/anion materials. The synergism of the potentially tridentate bridging triazolate and the effectiveness of the anionic components $X^{n-}$ in adopting bridging modes provides complex connectivity patterns and higher dimensional materials. Thus, of the compounds of this study, only [Zn(trz)Br] (**2**) is two-dimensional, while the remainder are three-dimensional.

The structural chemistry is complex, with both the identity of the metal and of the anion $X^{n-}$ acting as significant structural determinants. This observation is reinforced by the range of component substructures revealed by the materials of this study: clusters, rings, cages, chains, layers, and even three-dimensional frameworks. While only four zinc-containing phases are reported, the variability in coordination polyhedra is demonstrated by the tetrahedral, trigonal bipyramidal, and octahedral sites embedded in the structures. The anions $X^{n-}$ can also adopt a variety of bridging or terminal coordination modes, and the M−X−M and M−O−E (E = N, S) angles are quite "soft". While these factors provide a rich structural chemistry, they also contribute to the absence of predictability in the design of new materials.

The structural and compositional complexity of the metal−triazolate system can be further enhanced by the synthetic conditions exploited in their isolation. The hydrothermal domain is itself complicated, with variables such as time, temperature, stoichiometries of reactants, pH, nucleation and growth rates, starting materials, etc., requiring careful navigation. However, what is evident from this study and others in the emerging field of metal−polyazaheterocycle chemistry is the certainty that huge numbers of materials with unusual, unprecedented, and inconceivable structures remain to be discovered. Furthermore, as representative of the important class of organic/inorganic hybrid materials, the metal−triazolates exhibit a range of composite physical properties which may be amenable to tuning for applications to sorption, optical materials, and magnetism.

As an example of potentially useful physical properties, the open-framework structure of [Zn(trz)F]·$H_2O$ suggested potential microporosity. The dehydrated material [Zn(trz)F] is indeed microporous, exhibiting type I isotherms for sorption of $H_2$, $N_2$, and MeOH. Furthermore, the photoluminescence associated with many $d^{10}$ complexes encouraged us to study the optical properties of the materials of this study. However, only [Zn(trz)Cl] exhibited photoluminescence, presumably arising from a ligand $\pi-\pi^*$ transition.

**Acknowledgment.** This work was funded by a grant from the National Science Foundation, CHE-0604527. We thank Dr. Damian G. Allis for assistance with the DMol$^3$ calculations. We are also grateful to Prof. Joseph Chaiken for helpful discussions on the luminescence spectroscopy.

**Supporting Information Available:** Crystallographic files in CIF format for compounds **1**−**10**, TGA profiles for compounds **2**, **3**, **6**, and **8**−**10**, thermodiffraction profiles for **3**−**5** and 7, IR spectra for **5**·3$H_2O$, a BET $H_2$ isotherm of [Zn(trz)F], excitation and emission spectra for 1,2,4-triazole, and emission decay traces and experimental fits for [Zn(trz)Cl] at room temperature and at 77.4 K (Tables S.1−S.15). This material is available free of charge via the Internet at http://pubs.acs.org.

IC062269A